Available online at www.sciencedirect.com

ScienceDirect

Journal of Nutritional Biochemistry 134 (2024) 109711

Journal of Nutritional Biochemistry

RESEARCH PAPER

Treatment with 1.25% cholesterol enriched diet produces severe fatty liver disease characterized by advanced fibrosis and inflammation and impaired autophagy in mice

Alida Taberner-Cortés[a,#], María Aguilar-Ballester[a,#], Elena Jiménez-Martí[a,b], Gema Hurtado-Genovés[a], Rosa M. Martín-Rodríguez[a], Andrea Herrero-Cervera[a], Ángela Vinué[a], Susana Martín-Vañó[a], Sergio Martínez-Hervás[a,c,d], Herminia González-Navarro[a,b,d,*]

[a] Metabolic Diseases Group, INCLIVA Biomedical Research Institute, Valencia, Spain
[b] Biochemistry and Molecular Biology Department, Faculty of Medicine, University of Valencia, Valencia, Spain
[c] Endocrinology and Nutrition Department Clinic Hospital and Department of Medicine, University of Valencia, Valencia, Spain
[d] Metabolic Diseases Group, CIBER de Diabetes y Enfermedades Metabólicas (CIBERDEM), Instituto de Salud Carlos III, Madrid, Spain

Received 7 January 2024; received in revised form 15 July 2024; accepted 26 July 2024

Abstract

Nonalcoholic fatty liver disease (NAFLD) is reaching pandemic proportions due to overnutrition. The understanding of advanced stages that recapitulate the human pathology is of great importance to get a better mechanistic insight. We hypothesized that feeding of *WT* (C57BL) mice with a diet containing a high content of fat (21%), sugar (41.5%) and 1.25% of cholesterol (called from now on high fat, sucrose and cholesterol diet, HFSCD) will reproduce the characteristics of disease severity. Analysis of 16 weeks HFSCD-fed mice demonstrated increased liver weight and plasmatic liver damage markers compared with control diet (CD)-fed mice. HFSCD-fed mice developed greater hepatic triglyceride, cholesterol and NEFA content, inflammation and NAFLD activity score (NAS) indicating an advanced disease. HFSCD-fed mice displayed augmented hepatic total CD3+ T and Th9 lymphocytes, as well as reduced Th2 lymphocytes and CD206 anti-inflammatory macrophages. Moreover, T cells and anti-inflammatory macrophages correlated positively and inversely, respectively, with intrahepatic cholesterol content. Consistently, circulating cytotoxic CD8+ T lymphocytes, Th1, and B cell levels were elevated in HFSCD-fed WT mice. Hepatic and adipose tissue expression analysis demonstrated changes in fibrotic and metabolic genes related with cholesterol, triglycerides, and fatty acid synthesis in HFSCD-fed WT. These mice also exhibited reduced antioxidant capacity and autophagy and elevated ERK signaling pathway activation and CHOP levels. Our results indicate that the feeding with a cholesterol-enriched diet in WT mice produces an advanced NAFLD stage with fibrosis, characterized by deficient autophagy and ER stress along with inflammasome activation partially via ERK pathway activation.

Keywords: NAFLD; Inflammation; Metabolism; Cholesterol; Stress pathways.

Abbreviations: AUC, area under the curve; ALT, alanine aminotransferase; ANOVA, analysis of variance; AST, aspartate aminotransferase; BW, body weight; CD, control diet; CHOP, C/EBP homologous protein; ER, endoplasmic reticulum; FBS, fetal bovine serum; GTT, glucose tolerance tests; HCC, hepatocellular carcinoma; HDL, high density lipoprotein; HFD, high fat diet; HFSCD, high fat, sucrose and cholesterol diet; IR, insulin resistance; ITT, insulin tolerance tests; MCD, methionine choline deficient; NAFLD, nonalcoholic fatty liver disease; NAS, Nonalcoholic fatty liver disease activity score; NASH, nonalcoholic steatohepatitis; NEFA, nonesterified fatty acids; ROS, reactive oxygen species; RT, room temperature; SM-α-actin, smooth muscle α-actin; WT, wild-type mice.

On behalf of all coauthors: All coauthors have read and approved submission of the manuscript to *Journal of Nutritional Biochemistry.* The content of the manuscript is original neither has been published nor is under consideration for publication by any other journal. All coauthors have nothing to disclose. No use of generative AI or AI-assisted technologies during the analysis of data or the writing of the manuscript has been done. All authors meet the criteria for authorship and have approved the order of authors listed in the manuscript.

* Corresponding author at: Department of Biochemistry and Molecular Biology, Faculty of Medicine, Avenida Blasco Ibáñez, 15, 46010, Valencia, Spain.
E-mail address: herminia.gonzalez@uv.es (H. González-Navarro).
# Equal contribution.

https://doi.org/10.1016/j.jnutbio.2024.109711

1. Introduction

Chronic liver diseases are one of the main contributors to morbimortality and the tenth cause of death world-wide [1–3]. Among these, nonalcoholic fatty liver disease (NAFLD) stands out in terms of prevalence as it reaches pandemic proportions caused by the acquisition of sedentary life-style patterns and overnutrition that promote the development of the metabolic syndrome [2]. NAFLD is characterized by a complexity in its physiopathology which includes tissue metabolic dysfunction, hepatic fibrosis, and inflammation. Investigation in mouse models fed with high-cholesterol content diets might contribute to a better understanding of the disease as these can be clinically relevant since recapitulate key features of critic stages of the human pathology.

The overnutrition produces an excessive metabolic cell load in hepatic cells and adipocytes which promotes insulin resistance (IR) and dyslipidemia. Metabolic changes associated with high insulin levels and the anabolic overload provokes endoplasmic reticulum (ER) stress due to the accumulation of fatty acids that are unable to be either oxidized or enter in the lipid synthesis. These changes lead to the generation of toxic metabolic intermediates such as diacylglycerol and ceramide that activate MAPK stress pathways and secretion of inflammatory mediators. Deficient hepatic fatty acid oxidation hence becomes uncoupled with mitochondrial functioning which produces reactive oxygen species (ROS) [4]. Thus, at initial stages of NAFLD the liver keeps metabolic homeostasis, and the disease remains asymptomatic. But the accumulation of toxic intermediates and the stress pathway activation produce proinflammatory mediators and cells such as IL17 and IFNγ cytokines [5,6] and Th17 and CD8+T lymphocytes which promote liver damage and fibrosis [7]. Hepatic fibrosis is determinant for organ survival as the fibrotic scar replaces the hepatocytes which can lead to cirrhosis and hepatocellular carcinoma (HCC) [8,9]. Current most effective treatments to prevent these hepatic complications are based on the amelioration of the metabolic risk factors such interventions to reduce lipid levels, body weight loss, diabetes control, and exercise [4]. Despite of these, the prevalence remains unacceptably high.

Studies in animal models have provided important insights regarding molecular mechanisms accelerating NAFLD. Obesogenic high-fat containing diets, representing a total caloric intake between 45 and 75% from fat, have been shown to induce metabolic syndrome and NAFLD in mice which stem mostly from the obesity-mediated metabolic dysfunction [10]. On the other hand, NAFLD mouse models fed with a high-cholesterol rich high fat diet (HFD) during 16–20 weeks have been shown to induce liver damage, activation of immune and hepatic stellate cells (HSC) as well as mitochondrial dysfunction. These later diets seem to generate more advanced disease with enhanced fibrosis and inflammation with phenotypes closely related to human nonalcoholic steatohepatitis (NASH) [11]. These findings are also consistent with mounting clinical evidence indicating that the severity in NASH patients, which are not obese, associates with hepatic free cholesterol accumulation [12]. It is therefore of interest to determine how a high content cholesterol diets, in the context of overnutrition, promote hepatic advanced inflammatory and fibrotic stages.

Based on these previous studies we aimed to develop a human NAFLD model encompassing a proinflammatory phenotype and fibrosis. To this end, a diet containing high levels of cholesterol, fat, and sucrose (21 % of fat, 41.5 % of sucrose, and 1.25 % of cholesterol), called from now on a high fat, sucrose, and cholesterol diet (HFSCD) was designed and employed in this research. This diet was hypothesized to boost disease and recapitulate advanced stages of NASH characterized by fibrosis and inflammation. The study comprised metabolic and signaling pathway analysis and disease parameters (NAS score, fibrosis and hepatic lipid content) determinations. As a novelty in this study, we also characterized intrahepatic macrophage and T cell content as well as hepatic and systemic inflammation in relation to lipid accumulation.

Table 1
Composition of the customized Western-type HFSCD enriched in 21% of fat, 41.5% sucrose, and 1.25% of cholesterol.

Ingredients	g/Kg
Casein	195
DL-Methionine	3
Maltodextrin	75
Sucrose	405,36
Cellulose	50
Vitamin premix, AIN93G	10
Mineral premix, AIN93G	35
Calcium carbonate	4
Choline Cl	0
Cholesterol	12,5
Food dye, Green	0,1
BHT (antioxidant)	0,04
Butter fat, anhydrous	210
Proximate contents	%
Crude protein	17,2
Crude fat	21
Crude fiber	5
Crude ash	3,4
Dextrin	7,4
Sugar	41,5

2. Materials and methods

2.1. Mouse and diets

All mice used were housed in the animal facility of the Faculty of Medicine, University of Valencia. Sample size was calculated based on previous data (a priori test) using GPower 3.1 program. Wild-type mice (C57BL/6J background) (n=30) were fed a regular control diet (CD, Teklad Global Rodent Diets 6,5% fat; Teklad, Envigo, Barcelona, Spain) until the 8 weeks of age and then half of them were randomly assigned by experimentation personnel to the control group, which were mice fed during 16 more weeks with the CD, or to the experimental group, which consisted of mice fed with an experimental diet for 16 more weeks to induce characteristics of human NASH. The newly designed and customized experimental diet was based on the previous Western Diets [13] and as mentioned before with a 21% fat, 41.5% sucrose and 1.25% of cholesterol which was a modification of TD88137 (Table 1, Table A.1), HFSCD (S9052-E0123, SSNIFF, Germany). Mice had free access to water, were under temperature- and humidity-controlled conditions (22 ± 1°C, 40–45 %) and with 12h light-dark cycles in a conventional animal facility. Analysis was performed in male mice. Animal procedures were approved by the Ethical Committee of Experimental Research of University of Valencia (approval number 2020/VSC/PEA/00028) in which humane endpoints were stablished and followed the 2010/63/EU directive from the European Parliament.

2.2. Plasmatic measurements, body and liver weight, fat mass distribution and metabolic studies

Metabolic measurements were performed in isolated EDTA-preserved plasma from whole-blood of mice fasted overnight. Plasma analysis included triacylglycerol, total cholesterol, non–HDL-cholesterol, HDL-cholesterol (Wako Diagnostics, Mountain

View, CA, USA), nonesterified fatty acids (NEFA, Sigma St. Louis, MI, USA) and ALT and AST activities as reported [14]. Glucose tolerance tests (GTT) and insulin tolerance tests (ITT) were performed in overnight- and 4h-fasted mice, respectively as described [14]. Glucose (2g/Kg of body weight) and insulin (0.5 U/Kg of body weight) were injected in fasted mice and the levels of glucose for both tests and insulin for the GTT test were measured using a glucometer (Ascensia Elite, Bayer, Sant Joan Despí, Spain) and an ELISA assay (Enzyme-Linked ImmunoSorbent Assay, Crystalchem, Zaandam, Netherlands). For comparison purposes, the Area Under the Curve (AUC) parameter generated with the glucose (AUCglucose) and insulin (AUCinsulin) values at different time-points, was calculated. For liver and fat relative weight determinations these organs were dissected from mouse bodies, weighed, referred to total BW and expressed as percentage. Fat distribution was referred to total fat and expressed as percentage.

2.3. Hepatic lipid content and oxidative stress determinations

For hepatic content of triglycerides between 90 and 120 mg of liver tissue were digested followed by a saponification in ethanolic potassium hydroxide [15] to generate glycerol which was determined by an enzymatic reaction (Free Glycerol Reagent, Sigma) and converted into triglyceride concentration. For cholesterol and NEFA content 100 mg of liver was used to extract lipids. NEFA was measured using the commercial kit mentioned in 2.2. Free Cholesterol was extracted using the Folch method [16] and measured using UHPLC-PDA-MS/MS. Liquid chromatography-mass spectrometry detection was performed on a liquid chromatography UHPLC apparatus (Shimadzu, LCMS-8040) coupled to a tandem mass spectrometry (MS/MS) triple quadrupole equipped with electrospray ionization (ESI) ion source (Shimadzu, Kyoto, Japan), a platform of INCLIVA. For oxidative stress reduced and oxidized glutathione (GSH, GSSG) and malondialdehyde (MDA) determinations were done employing Glutathione colorimetric detection kit (Invitrogen, EIAGSHC) and Malondialdehyde (MDA) Colorimetric Assay (Ebiosciences, E-BC-K025-S) respectively.

2.4. Liver histopathology determinations

Histologic determinations were performed in cross-sections from mouse livers washed with PBS, fixed with 4% paraformaldehyde/PBS and paraffin embedded [15]. Liver pathology was assessed by determining the steatosis, hepatocellular ballooning, and lobular inflammation in hematoxylin-eosin stained sections which were employed to calculate the NAS score as reported [15]. Connective tissue and collagen contents in hepatic cross-sections were detected with a Ponceau S-picric acid staining solution and with Masson's trichrome staining (BioOptica, Milan Italy) respectively. Hepatic infiltrated CD3+ T cell detection was performed by immunofluorescence in cross-sections treated for antigen retrieval with sodium citrate buffer, 10 mM pH 5.0, at high temperature and pressure. After blocking with 5% fetal bovine serum (FBS), sections were incubated overnight at 4°C with a rabbit antihuman CD3 antibody (DAKO, Santa Clara, CA, USA) and then with an antirabbit AlexaFluor 488 secondary antibody (Invitrogen) 1h at room temperature (RT). Sections were mounted with Slow Fade reagent media (Sigma) and a cover slip. Detection of activated HSC, consisted of an anti-SM-α-actin immunohistochemistry which employed an incubation (overnight at 4°C) with a primary monoclonal antibody (1/20, A5691Sigma) conjugated with alkaline phosphatase, followed by a reaction development with Fast Red (Sigma) substrate and mounting with glycerol gelatin (GG1, F-4648 Sigma) and cover slip for microscope analysis. Contents of connective tissue, collagen and SM-α-actin were expressed as percentages of area occupied by the marker relative to total hepatic area. T cell content was expressed as number of cells/μm^2 of hepatic area.

For p62/SQSTM1 and Ki67 immunostainings, paraffin-embedded cross-sections were treated for antigen retrieval and blocking as before followed by inactivation of endogenous peroxidase activity (3% in water for p62/SQSTM1 and, 0,3% in methanol for Ki67). For Ki67 detection, sections were also treated for endogenous biotin blocking with avidin-biotin kit solution (DAKO). Sections were then incubated overnight at 4°C with primary antibodies (1/100 dilution of a rabbit polyclonal anti-p62/SQSTM1, PA5-27247 Invitrogen Thermofisher, Waltham, MA, USA; prediluted rabbit monoclonal anti Ki-67 (SP6) MAD-000310QD-7 Master Diagnostica, Vitro SA, Sevilla, Spain). Sections were incubated 1 h at RT with HRP-conjugated goat antirabbit IgG antibody (1/300 P0488 DAKO, Berlin, Germany) for p62 or with a biotinylated goat antirabbit antibody (65-6140 1/500 Invitrogen, Thermofisher, Waltham, MA, USA) followed by 7 min incubation with Streptavidin-HRP (1/500 Ab7403 ABCAM Cambridge, UK) for Ki67. Detection of immunocomplexes was done with diaminobenzidine (DAB BUF021A AbD SEROTEC, Bio-Rad Laboratories, UK). Immunostainings were followed by counterstaining with hematoxylin and nonaqueous mounting with Eukitt (A10500, Deltalab, Barcelona, Spain). Images were captured with camera coupled to an optical microscope with a built-in camera Leica DMD108 Digital Microimaging Device (Leica Microsystems, Wetzlar, Germany) and analyzed with the help of a software (Image Processing and Analysis in Java, NIH). All quantifications were performed using Image J/Fiji software (Fiji, ImageJ-win64, NIH, Bethesda, MD, USA). Quantifications were performed to display percentage of area occupied by p62/SQSTM1 relative to hepatic area or as number of cells relative to hepatic area for Ki67.

2.5. Flow cytometry analysis of circulating leukocytes and hepatic macrophages and lymphocytes

For analysis of circulating leukocytes heparinized whole blood was incubated with antibodies using different flow cytometry protocols. For monocyte determination 10 μL of blood were incubated for 30 min at RT with 1 μL of CD45-FITC (553080, BD Pharmingen, Franklin Lakes, NJ, USA), Ly6C-PerCP (560525, BD), and CD115-APC (135510, eBiosciences), which were used to quantify total CD115+, patrolling Ly6C^{low} and proinflammatory Ly6C^{hi} macrophages. Circulating T and B lymphocytes, neutrophils and natural killer (NK) cells were analyzed in 10 μl of blood incubated as before with 5 μl of Brilliant stain buffer (563794, BD) and with 1 μL of: anti-CD3e-APC (553066, BD), anti-CD4-FITC(562891, BD), anti-CD8a-BV510 (563068, BD) anti-CD69-PE (553237, BD), anti-CD19-VioBlue (130-112-041 Miltenyi), anti-Ly6G-APCVio700 (130-119-126, Miltenyi) and NK1.1-PerCPVio700 (Miltenyi, 130-117-773). For identification of T helper (Th) cells 30 μL of blood were incubated as before with 1μL of anti-C-C chemokine receptor (CCR)4 (CD194)-BV421 (131217, BioLegend), anti-CD4-FITC (130-102-541, Miltenyi), anti-CXC chemokine receptor (CXCR)3 (CD183)-APC (17-1831-80, eBioscience) and anti-CCR6(CD196)-PEVio770 (130-103-818, Miltenyi). For regulatory T (Treg) cells, 50 μL of blood were stained with 2.5 μL of anti-CD4-BV421 (562891, BD) and 5 μL of anti-CD25-APC (130-108-997, Milteny) antibodies, followed by 30 min incubation with Foxp3 fixation/permeabilization buffer (Kit FoxP3 Staining Buffer Set, 130-093-142, Miltenyi) and a 30 min incubation with 5μL of anti-Foxp3-PE (130-093-014, Miltenyi).

For hepatic macrophage and lymphocyte characterization between 200 and 250 mg of tissue was digested with 4,5 mg/ml type I collagenase (LS004194, Worthington, Lakewood, NJ, USA) diluted in RPMI media with 10% of fetal bovine serum (FBS)

at 37°C for 30 min under manual agitation. After filtering with a 40μm nylon filter (431750, Corning, NY USA), cells were washed and collected, resuspended in red blood cell lysis buffer (555899, BD BIOSCIENCES) and fixed with Zombie Aqua fixable viability kit (BioLegend, San Diego, CA, USA). Unspecific binding was avoided by an incubation with 200μl of FcR Blocking Reagent Mouse (Miltenyi) and then cells were stained for macrophage and T lymphocytes characterization (30 minutes at room temperature, RT). For macrophage staining, cells were incubated with a mix of antimouse F4/80-APC (MCA497APTC, AbD-Serotec), antimouse CD11c-PE (12-0114-81, eBioscience, San Diego, CA, USA), and antimouse CD206-AlexaFluor488 (MCA2235A488T, AbD Serotec) antibodies. Analysis was set to determine total F4/80+, proinflammatory F4/80+CD11c+CD206− and anti-inflammatory F4/80+CD11c−CD206+ macrophages. For lymphocyte analysis, cells were stained with the antibodies indicated above for CD3+, CD4+, CD8+ and CD4+Th subsets.

All protocols were followed by an incubation with red blood cells lysing solution (BD Biosciences) for 15–20 min and analyzed using Fortessa Flow cytometer (BD LSR Fortessa Xnd 20; BD Biosciences, Franklin Lakes, NJ USA) and BD FACSDiva software (BD Biosciences, Franklin Lakes, NJ USA).

2.6. Western blot analysis

Protein extracts were obtained by homogenizing 30 mg of snap-frozen liver and adipose tissue with manual homogenizers in the presence of TNG buffer (50mM Tris-HCl pH 7.5, 200mM NaCl, 1% Tween-20 y 0.2% NP-40) supplemented with Complete Mini cocktail (ROCHE, Mannheim, Alemania), 100mM ß-glycerolphosphate (SIGMA), 100mM phenylmethylsulfonyl fluoride (PMSF, Roche), 200μM NaVO3 (Sigma) and phosphatase inhibitors PhosSTOP (ROCHE). Tissue lysates underwent three freeze-thaw cycles, using liquid N_2 and a 37°C water bath, and vortex mixing. About 25–100 μg of protein extracts were prepared in Laemmli buffer (5 min 95°) and subjected to 12% w/v polyacrylamide gel electrophoresis and western blot. Membranes were blocked with 5% BSA/PBS1X-0,01% Tween 20 and incubated at overnight 4°C with the following primary antibodies: a mouse monoclonal anti-phosphoERK antibody (1/500 sc-7383 Santacruz Biotech, Santa Cruz, CA, USA) a rabbit monoclonal anti-phosphoSAPK/JNK (1/500 9251, Cell Signaling, Danvers, MA, USA), a rabbit polyclonal IgG anti-phosphop38 (1/200 sc-17852-R Santacruz Biotech, Santa Cruz, CA, USA), a rabbit monoclonal anti-CHOP 9251 (1/500 5554, Cell Signaling), a rabbit polyclonal anti-ERK2 (1/200 sc-154 SantaCruz), a rabbit monoclonal anti-JNK (1/500 9252 Cell Signaling), a rabbit polyclonal IgG anti-p38 (1/200 sc-535, Santacruz Biotech, Santa Cruz, CA, USA), a rabbit anti-phospho(Thr172)AMPK (1/500 2531, Cell Signaling), a rabbit anti-AMPK (1/500 2532, Cell Signaling), a rabbit anti-NPLR3 (1/100 15101 Cell Signaling), a rabbit anti-phospho(Ser563) Hormone sensitive lipase (HSL) (1/100 4139 Cell Signaling), a rabbit anti-HSL (1/100 4107 Cell Signaling), a rabbit Anti-NPLR3 (1/100 15101 Cell Signaling), and a mouse monoclonal anti-β-actin (1/1000 A5441, Sigma). The immunocomplexes were detected with HRP-conjugated secondary antibodies, a goat antirabbit IgG-HRP (P0488, DAKO) and a goat antimouse IgG-HRP (P0447, DAKO) (1/2000) followed by chemiluminescent detection using an ECL Plus detection kit (ThermoFisher) using a Luminescent Image Analyzer LAS4000 (FUJIFILM, Tokio, Japan). Quantifications of protein levels were done on images using FIJI software. For normalization unphosphorylated protein or β-actin levels were used. All antibodies for western blot were acquired and used after checking that validation was performed by manufacturer company.

2.7. mRNA expression studies by quantitative real-time PCR

Total RNA was obtained from liver and adipose tissue samples using TRIzol reagent (Invitrogen, Thermofisher Scientific, Waltham, MA, USA). Between 0.5-1μg of RNA were reverse transcribed with the Maxima First-Strand kit (Thermofisher Scientific, Waltham, MA, USA) and the mRNAs for the target genes were amplified using the Luminaris Color HiGreen High ROX qPCR Master Mix (Thermofisher Scientific, Waltham, MA, USA) on a 7900 FastSystem thermal cycler. Results were analyzed with the formula $2^{-\Delta\Delta Ct}$ using the mRNA levels of the *Cyclophilin* gene for normalization and CD-fed mouse liver mRNA levels for relativization. The primer sequences were obtained from the PrimerBank data base (Massachusetts General Hospital, Harvard University) and are listed in Table A.2 and A.3.

2.8. Statistical analysis

Quantitative variables are shown as single data points and bar graphs with mean ± SEM. The sample size was 20 mice which was calculated using GPower 3.1 using *a priori test* and previous published experimental data. All mouse sample replicates were obtained from individual mice and were assigned to control or experimental group randomly. All data obtained were analyzed by observers blinded to treatments. The exclusion criteria for data were out of range of the standard curve or samples that were lost during the experimentation. Outliers were identified with Grubbs's test. Data were analyzed for normal distribution using D'Agostino–Pearson, Kolmogorov-Smirnov or Saphiro-Wilk tests. Differences between two groups were evaluated with unpaired Student's t test (parametric) or Mann–Whitney U test (nonparametric test) for comparisons between two mouse groups and by two-way ANOVA for two variable comparisons. Correlations between quantitative variables were shown as single data points and significance was assessed by Pearson's (parametric) or Spearman (nonparametric) correlation analysis. Analysis of the different parameters were done by comparing HFSCD-fed and CD-fed mice. Statistical significance was set at $P \leq .05$.

3. Results

3.1. WT *mice fed a high sucrose fat and cholesterol rich diet characterization*

As expected, analysis of BW showed an increment in both CD and HFSCD compared with the same mice at the beginning of the study, but 16-weeks HFSCD-fed mice displayed reduced BW compared with 16-weeks CD-fed mice (Fig. 1A). However, liver weight was significantly higher in HFSCD-fed mice compared with CD-fed controls (Fig. 1B). No changes were seen in body fat mass between mouse groups (Fig. 1C, D). But fat distribution examination showed a nonsignificant slight increase in epididymal fat percentage and a significantly decreased percentage in mesenteric fat in HFSCD-fed mice (Fig. 1E). Mesenteric adipose tissue *Lep* mRNA levels were reduced (Fig. 1F) which was consistent with reduced depots of this tissue in HFSCD-fed *WT* mice. Interestingly, *Lep* mRNA levels positively correlated with % of mesenteric fat in all mice (Fig. 1G). Analysis of plasmatic lipid profile showed augmented total cholesterol levels in HFSCD-fed mice (Fig. 1H) with a slight not significant elevation in non-HDL-cholesterol and HDL-cholesterol levels (Fig. 1I, J). No changes in plasmatic triglyceride levels were seen (Fig. 1K) among groups while NEFA levels were reduced in HFSCD-fed mice (Fig. 1L).

No changes in glucose levels neither at the beginning of the study nor after the diets between mouse groups were seen

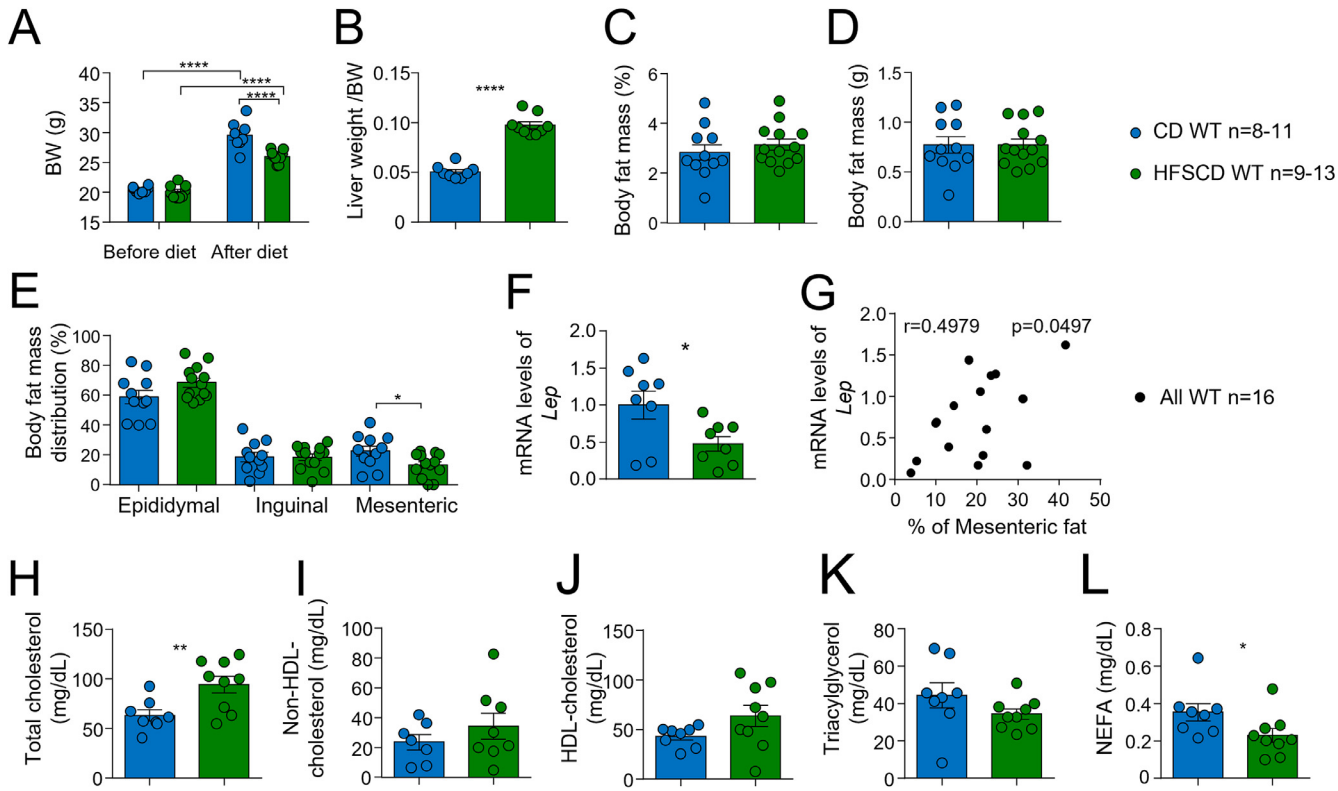

Fig. 1. HFSCD feeding of *WT* mice increases liver weight and circulating cholesterol levels but reduces NEFA blood levels. Body weight (A) and liver weight (B) expressed as percentage of total body weight in both mouse groups before and after 16 weeks of diet. Body fat mass expressed as percentage (C) and as absolute (D) number of total body weight and body fat mass distribution (E) expressed as percentage of total fat in both mouse groups. (F) *Lep* mRNA levels in mesenteric fat from both mouse groups. (G) Correlation between mesenteric fat *Lep* mRNA levels and % of mesenteric fat. Plasmatic levels of (H) total cholesterol, (I) non-HDL-cholesterol, (J) HDL-cholesterol, (K) triacylglycerol and (L) NEFA. Data is depicted as individual data points and with the mean±sem. Statistical analysis was performed using followed by Tukey's multiple comparison test (A) and Studentś t test (B, D-F, H-K), Mann-Whitney U test (C, L) and Pearson correlation coefficient (G). (* $P \leq .05$, ** $P < .01$ and **** $P < .0001$).

(Fig. 2A). GTT unexpectedly revealed a significant improvement in the glucose tolerance, measured as $AUC_{glucose}$ in HFSCD-fed mice compared with CD-fed mice (Fig. 2B, C) but insulin release measured with $AUC_{insulin}$ during the GTT was similar between mouse groups (Fig. 2D, E). Conversely, peptide C measurement during the GTT demonstrated decreased $AUC_{C\text{-}peptide}$ in HFSCD-fed mice (Fig. 2F, G) indicating decreased insulin secretion in this mouse group. Insulin sensitivity, examined with an ITT also showed decreased $AUC_{glucose}$ in HFSCD-fed mice (Fig. 2H, I).

These results indicate that *WT* mice fed a HFSCD unexpectedly develops reduced body weight, altered fat mass distribution despite no changes in total fat mass and improved glucose metabolism parameters. Moreover, HFSCD provoked an accumulation of circulating cholesterol levels while NEFA levels were reduced.

3.2. High sucrose, fat and cholesterol-rich diet induces fatty liver and fibrosis in WT mice

Regardless of the plasmatic levels of lipids, liver examination showed enhanced intrahepatic triacylglycerol, free cholesterol and NEFA contents in *WT* mice fed the HFSCD compared with CD-fed *WT* mice (Fig. 3A–C). Consistently, steatosis, lobular inflammation and ballooning degeneration were significantly augmented in HFSCD-fed *WT* mice which resulted in increased NAS score (Fig. 3D–G). Analysis of ALT and AST activities indicated liver damage in HFSCD-fed *WT* mice compared with controls (Fig. 3H, I). Cytokine mRNA expression analysis showed significantly increased levels of *Mcp1* and *Tnfa* (Fig. 3J, K) in HFSCD-fed *WT* mice and no changes in *Ifng* (Fig. 3L) indicating increased inflammation.

HFSCD-fed *WT* mice displayed augmented content of collagen (Fig. 4A), Ponceau S-stained fibrin connective tissue (Fig. 4B) and SM α-actin+ area (Fig. 4C). Further analysis through expression studies of genes involved in the fibrotic process showed elevated mRNA levels of *Timp1* and *Tgfb1* (Fig. 4F, G) and a nonsignificant diminished expression level of *Col1a1* gene (Fig. 4D). No differences were seen in *Mmp9* mRNA levels between mouse groups (Fig. 4E).

3.3. Fatty liver in WT mice fed a high sucrose, fat and cholesterol rich diet develops with systemic and hepatic inflammation

Progressive accumulation of intrahepatic lipids in fatty liver disease is characterized by activation of inflammatory pathways. Examination of total F4/80+ and proinflammatory F4/80+CD11c+ macrophages were alike between HFSCD- and CD-fed mice (Fig. 5A, Supplementary Fig. A1A, B). But anti-inflammatory F4/80+CD206+ macrophages were decreased in HFSCD-fed *WT* mice (Fig. 5B, C and Supplementary Fig.A1A, B) suggesting higher inflammatory status. Consistently, the total infiltration of CD3+T cells determined by immunofluorescence was significantly elevated (Fig. 5D). Interestingly, there was an inverse correlation between F4/80+ macrophage content and triacylglycerol (Supplementary Fig. A2A) as well as an inverse correlation between anti-inflammatory F4/80+CD206 macrophage subpopulation with triacylglycerol, free cholesterol and NEFA (Supplementary Fig. A2C, G, K). In addition, free cholesterol content positively correlated with CD3+ T

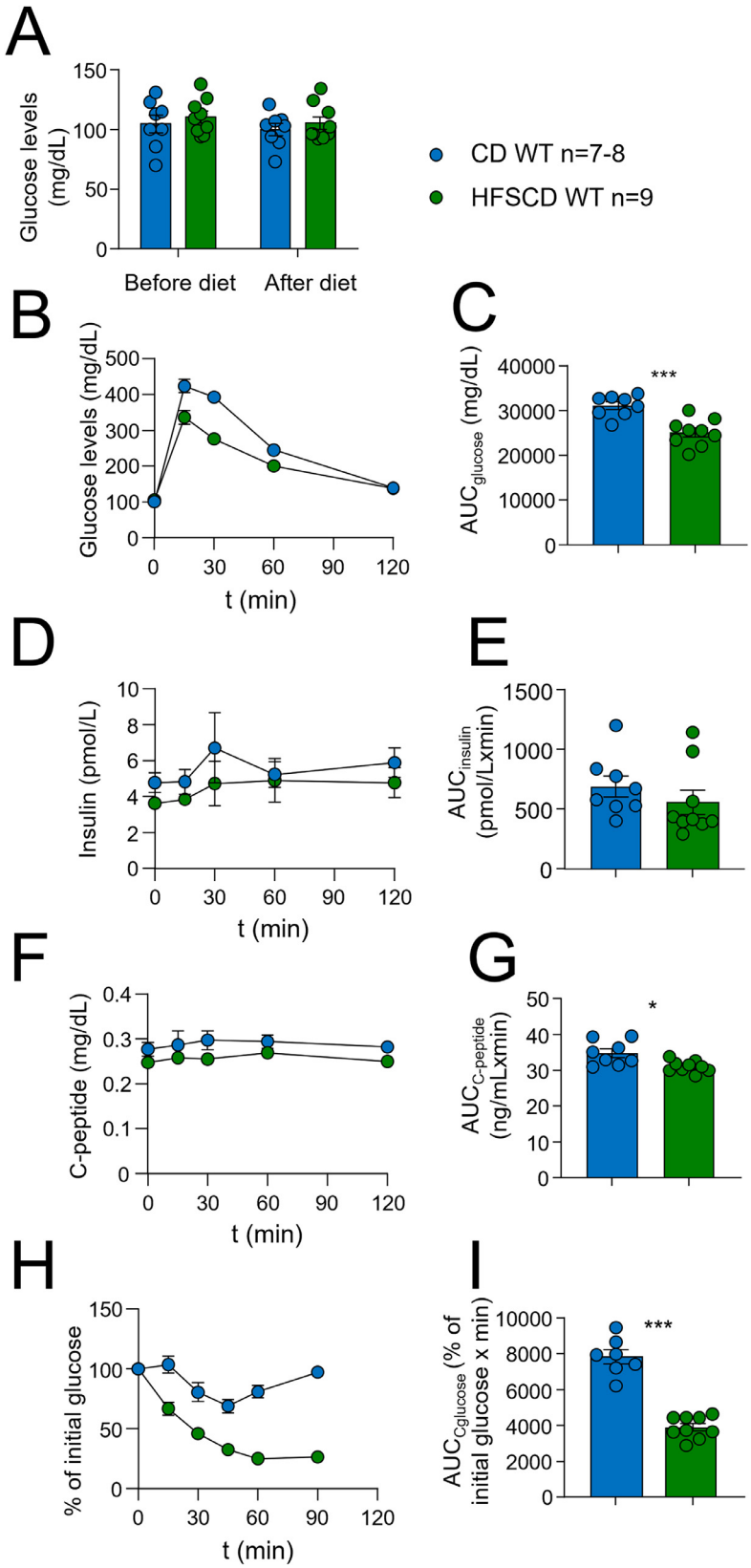

Fig. 2. Metabolic characterization of *WT* mice placed 16 weeks on CD and HFSCD. (A) Plasmatic fasting glucose before and after the diet in *WT* mice fed both diets. Plasmatic (B) glucose, (D) insulin and (F) C-peptide levels at the different time points during the GTT. These were used to calculate the $AUC_{glucose}$ (C), $AUC_{insulin}$ (E) and $AUC_{C\text{-}peptide}$ (G), in CD- and HFSCD-fed *WT* mice. (H) Plasmatic glucose levels (in percentages relative to the initial glucose levels) during the ITT and the $AUC_{glucose}$ (I) parameters for the two mouse groups. Data is depicted as individual data points and with the mean±sem. Statistical analysis was performed using two-way ANOVA followed by Tukey's multiple comparison test (A), Studentś t test (C, E, G) and Mann-Whitney U test (I). ($^{*}P<.05$ and $^{***}P<.001$).

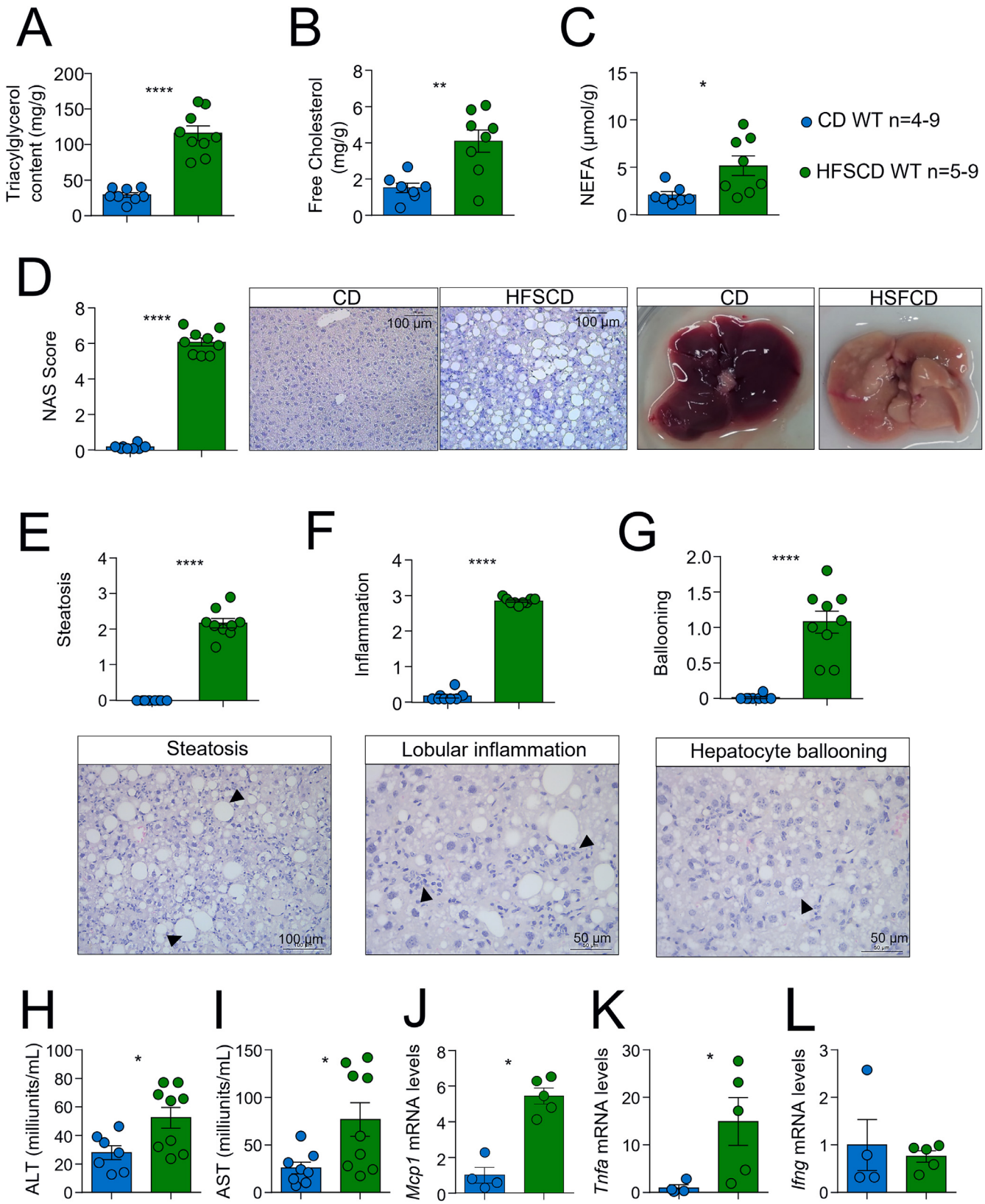

Fig. 3. *WT* feeding for 16 weeks with a HFSCD produced hepatic steatosis and liver damage. Intrahepatic (A) triacylglycerol, (B) free cholesterol and (C) NEFA content in both *WT* mice fed CD and HFSCD. (D) NAS score calculated with the parameters of (E) steatosis, (F) lobular inflammation and (G) hepatocyte ballooning determined in hepatic cross-sections. Representative images hepatic cross-sections and whole liver for both mouse groups are shown next to the NAS score. Black arrows point to steatosis, lobular inflammation and hepatocyte ballooning in representative images which are displayed below to the corresponding quantifications. Plasmatic levels of (H) ALT and (I) AST activities in both dietary regimens. mRNA levels of (J) *Mcp1*, (K) *Tnfa*, and (L) *Ifng* genes in both mouse groups. mRNA expression levels were normalized with *Cyclophilin* and relativized to CD-fed mouse mRNA levels. Data is depicted as individual data points and with the mean±sem. Statistical analysis was performed using Studentś t test (A–C, E–I) and Mann-Whitney U test (D, J–L). ($^{*}P<.05$, $^{**}P<.01$ and $^{****}P<.001$).

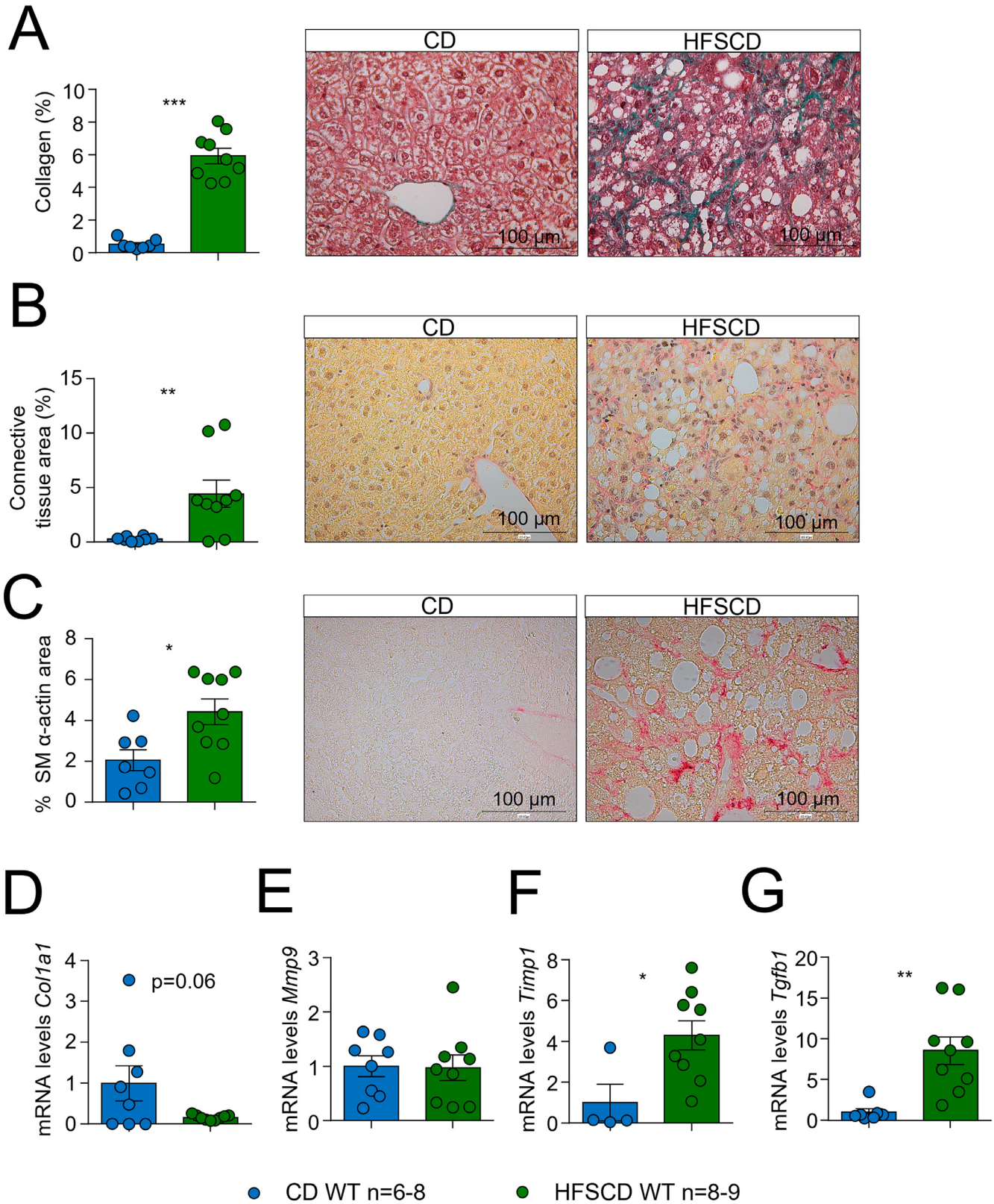

Fig. 4. HFSCD-fed *WT* mice develop fibrosis and altered fibrotic gene expression. Area percentages of (A) collagen detected with Masson's trichrome staining, (B) connective tissue detected with ponceau S-picric acid solution and (C) SM-α-actin staining for hepatic stellate cell (HSC) activation. Representative images of the of the staining's are shown next to the quantifications for both dietary regimens. mRNA levels of (D) *Col1a1*, (E) *Mmp9*, (F) *Timp1* and (G) *Tgfb1* genes. mRNA expression levels were normalized with *Cyclophilin* and relativized to CD-fed mouse mRNA levels. Data was represented as individual data points and with the mean±sem. Statistical analysis was performed using Studentś t test (B-E) and Mann-Whitney U test (A, G, F). ($^{*}P<.05$, $^{**}P<.01$ and $^{***}P<.0001$).

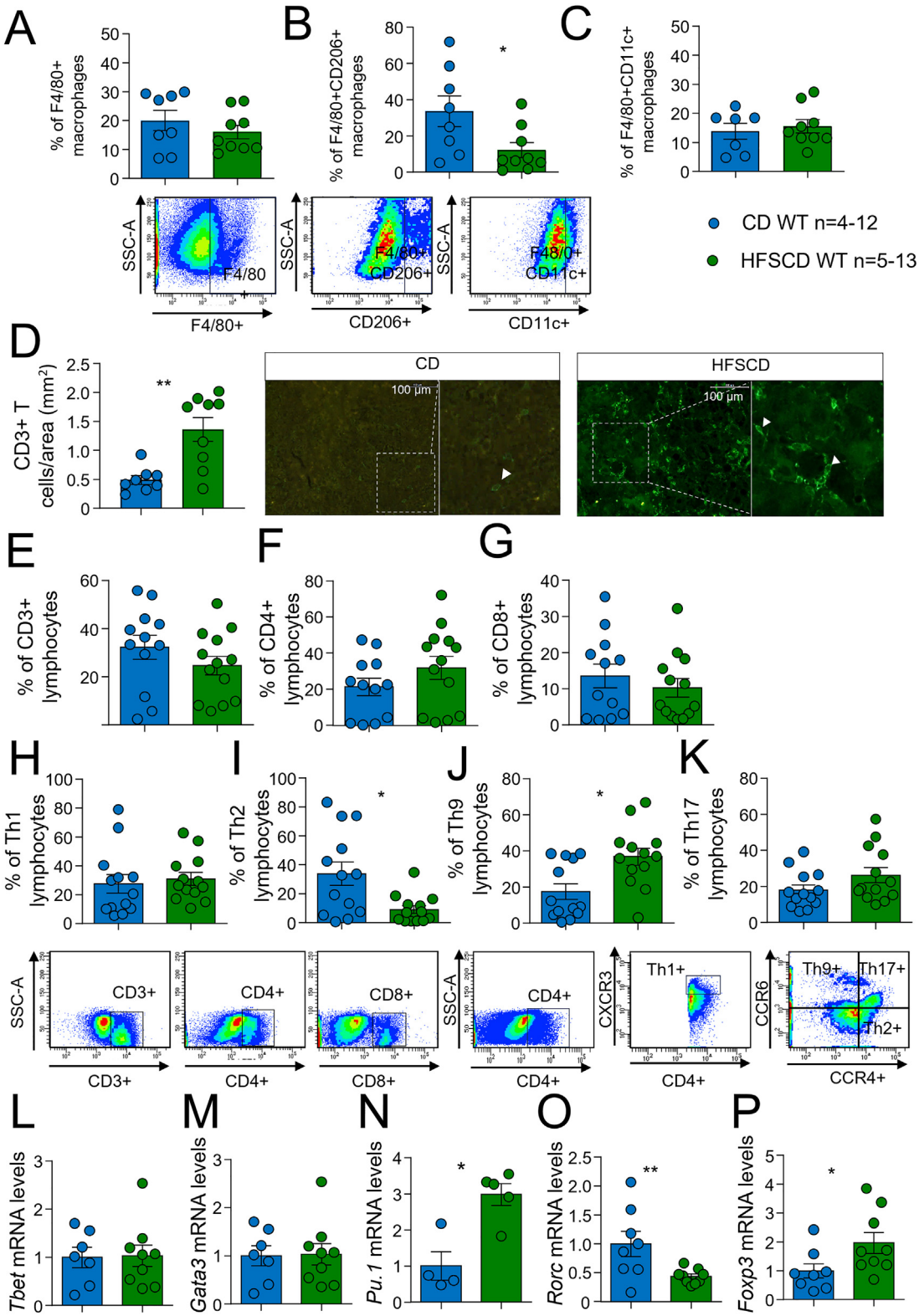

Fig. 5. HFSCD-fed WT mice display hepatic inflammatory profile and altered inflammatory transcription factors. Percentage of (A) total F4/80+, (B) anti-inflammatory F4/80+CD206+ and (C) proinflammatory F4/80+CD11c+ macrophages in alive cells from hepatic stromal vascular fractions (SVF) determined by flow cytometry. Representative flow cytometry plots displaying the gating strategy for the different populations are displayed below the quantifications. (D) Content of CD3+T cells, expressed as number of cells per area (in mm^2), in the liver of both mouse groups. Hepatic (E) CD3+, (F) CD4+ and (G) CD8+ T lymphocytes referred to tissular total lymphocytes represented as percentage of total lymphocytes. Analysis of the percentages of (H) CD4+CXCR3+ Th1, (I) CD4+CCR4+CCR6-Th2, (J) CD4+CCR4-CCR6+Th9 and (K) CD4+CCR4+CCR6+Th17 populations represented as percentage of total CD4+ T lymphocytes. mRNA levels of (L) *Tbet*, (M) *Gata3*, (N) *Pu.1*, (O) *Rorc* and (P) *Foxp3* transcription factors in liver from both groups of mice. mRNA levels were normalized with *Cyclophilin* mRNA levels and relativized to CD-fed *WT* mouse levels. Data was represented as individual data points and with the mean±sem. Statistical analysis was performed using Student's t test (A, B, D–H, K, M–P) and Mann-Whitney U test (C, I, J, L). ($^{*}P<.05$ and $^{**}P<.01$).

cell number (Supplementary Fig. A2H). These results suggested an association between intrahepatic lipid accumulation, especially of free cholesterol, and proinflammatory cell content.

Further hepatic lymphocyte characterization by flow cytometry indicated a similar relative percentage of CD3+, CD4+ and CD8+ T cells (Fig. 5E–G and Supplementary Fig. A1C, D). But CD4+ subset determinations demonstrated a reduced percentage of CCR4+CCR6-Th2 cells and augmented CCR4-CCR6+Th9 lymphocytes in HFSCD-fed WT mice compared with CD-fed WT controls (Fig. 5I, J and Supplementary Fig. A1E, F). No changes between mouse groups were seen in CXCR3+Th1 or in CCR4+CCR6+Th17 lymphocytes (Fig. 5H, K and Supplementary Fig. A1E, F).

Expression analysis in liver of transcription factors determinant for CD4+T cell subset differentiation showed similar mRNA levels of *Tbet* and *Gata3* between mouse groups (Fig. 5L, M). But decreased *Rorc* and augmented *Foxp3* mRNA levels were seen in HFSCD-fed *WT* mice (Fig. 5O, P). Notably, consistent with increased Th9 lymphocytes their key transcription factor *Pu.1* gene expression was significantly increased in HFSCD-fed *WT* mice (Fig.5N).

Circulating levels of leukocytes showed no changes in lymphocytes or granulocytes between CD- and HFSCD-fed *WT* mice (Fig. 6A and Supplementary Fig. A3A, B). By contrary, HFSCD-fed *WT* mice exhibited decreased circulating total CD115+ monocytes and proinflammatory CD115+Ly6C^{hi} monocyte subset while anti-inflammatory CD115+Ly6C^{low} monocytes were increased (Fig. 6A, B and Supplementary A3A, B). This result suggested a higher infiltration capacity of the total and proinflammatory monocytes and a reduced infiltration capacity of the anti-inflammatory monocytes from HFSCD-fed *WT* mice. Analysis of circulating lymphocytes and subsets in both mouse groups revealed, in HFSCD-fed *WT* mice, decreased CD4+ T cells, augmented cytotoxic CD8+ T cell subset but decreased CD8+CD69+ activated T cells and no changes in CD3+ T cells or other CD69+ activated T cell subpopulations (Fig. 6C–H and Supplementary Fig. A3C, D). Further analysis demonstrated higher percentages of CD4+CXCR3+Th1 and CD19+ B lymphocytes in HFSCD-fed *WT* mice (Fig. 6I, N and Supplementary Fig. A3E–H). CD4+CCR4+CCR6-Th2, CD4+CCR4-CCR6+Th9, CD4+CCR4+CCR6+Th17 and CD4+CD25+Foxp3+Treg cells remained unchanged between CD and HFSCD-fed *WT* mice (Fig. 6J–M and Supplementary Fig. A3E, F).

3.4. Fatty liver in WT mice fed a high sucrose, fat and cholesterol rich diet modulates metabolic genes

Pathologic hepatic lipid accumulation is expected to induce metabolic derangement; hence, hepatic key regulatory enzymes were examined. Determination of activated phosphoAMPK protein levels were alike between HFSCD- and CD-fed mice but total AMPK levels were increased in HFSCD-fed mice (Supplemental Figure A4A, B). Analysis of gluconeogenic genes showed a consistent reduction in *G6pase* mRNA levels in HFSCD-fed mice compared with those in CD-fed mice (Fig. 7A). No changes were seen in the *Pepck* mRNA levels or in the energetic metabolism regulator *Pgca1* (Fig. 7B, C). Lipid synthesis gene expression analysis demonstrated, in HFSCD-fed *WT* mice, reduced mRNA levels of the transcription factors *Chrebp, Lxr* and the enzyme *Fasn* (Fig. 7D, J, L), consistent with lipid synthesis inhibition and increased AMPK protein levels. Although *Pparg* levels were augmented (Fig. 7F). No changes in the mRNA levels of *Ppara, Acox* and *Srebf1* metabolic genes were seen between mouse groups (Fig. 7E, I, K). Regarding the lipid and lipoprotein transport genes the mRNA levels of the *Ldlr* were diminished while those of the fatty acid transporter *Cd36* were significantly augmented in HFSCD-fed *WT* mice (Fig. 7G, H) which was consistent with intrahepatic NEFA accumulation. In agreement with intrahepatic free cholesterol accumulation in HFSCD-fed mice, gene expression of *Srb1* was increased (Fig. 7O) and *Abca1* gene was reduced (Fig. 7P). The gene expression of the main cholesterol synthesis regulator *Hmgcr* was reduced (Fig. 7M) and the mRNA levels of *Abcg5* gene, relevant at preventing sterol hepatic accumulation, was augmented (Fig. 7Q). No changes were seen in *Ceh, Fxr* and *Cyp7a1* gene expression (Fig. 7N, R, S) among mouse groups.

Reduced mesenteric fat and leptin production and intrahepatic accumulation of NEFA suggest an enhanced adipose tissue lipolysis in HFSCD-fed *WT* mice, hence adipose tissue was next investigated. Analysis showed in HFSCD-fed *WT* mice elevated phosphoHSL/HSL protein ratio and augmented expression of *Plin* gene (Supplementary Fig. A5A, B, D) suggesting activated lipolysis. No changes in the mRNA levels of HSL gene *Lipe* (Supplementary Fig. A5C) were seen. Moreover, the mRNA levels of the other lipases *Pnpla2* and *Mgll* associated with the catabolism of lipid droplets and of the transcription factor *Cidea* (Supplementary Fig. A5E–G) were similar between mouse groups.

3.5. A high sucrose, fat and cholesterol rich diet impairs autophagy and promotes hepatocyte proliferation

NAFLD progression and hepatic cholesterol accumulation has been associated with oxidative and ER stress which encompass the dysregulation of several process such as apoptosis and autophagy. GSH levels were significantly decreased in HFSCD fed mice suggesting a lower ability to alleviate oxidative radicals (Fig. 8A left panel). By contrary, no changes were seen in the levels of GSSG or MDA for oxidized lipids between mouse groups (Fig. 8A, B). The analysis of the p62 (SQSTM1), a marker of accumulated autophagosomes and a deficient autophagy flux demonstrated increased content in HFSCD fed mice (Fig. 8C). Notably, CHOP protein, which is involved in ER stress-induced apoptosis cell death was also significantly enhanced in HFSCD-fed mice (Fig. 8D). On the other hand, ER stress and cholesterol crystals can induce inflammation through inflammasome. Accordingly, NLRP3 protein levels were elevated in HFSCD-fed mice (Fig. 8E).

Analysis of proliferation, a process indicative of NAFLD progression, in hepatic cross-sections also showed an increment in proliferative Ki67+ cells in the livers from HFSCD-fed mice compared with CD-fed WT mice (Fig. 8F).

3.6. A high sucrose fat and cholesterol rich diet increases activated ERK and modulates phosphatases gene expression

To evaluate the possible alteration of signaling pathways induced by the HFSCD, stress MAPK and MAPK phosphatases (MKP)/DUSP, which have been previously involved in fatty liver development, were analyzed.

Liver analysis showed increased activation of ERK, shown as increased phosphorylated form phosphoERK in HFSCD-fed mice compared with CD-fed mice (Fig. 9A). But, activated phosphoSAPK/JNK and phosphop38/p38 ratio levels were similar between both mouse groups (Fig. 9B). Gene expression analysis of *Mkp/Dusp* genes indicated an increased hepatic expression of *Dusp2, Dusp3, Dusp5, Dusp8, Dusp10* and *Dusp18* in HFSCD-fed but not in *Dusp1, Dusp6, Dusp12, Dusp16* and *Dusp22* mice (Fig. 9 D–N).

4. Discussion

NAFLD has become a main problem worldwide mainly due to overnutrition and sedentary life-style patterns in the population [3]. One key factor by which overnutrition induces severe inflammation and fibrosis, regardless of the steatosis degree, is the hepatic accumulation of free cholesterol. In the present investigation, we hypothesized that a diet enriched with 21% fat, 41.5% sucrose,

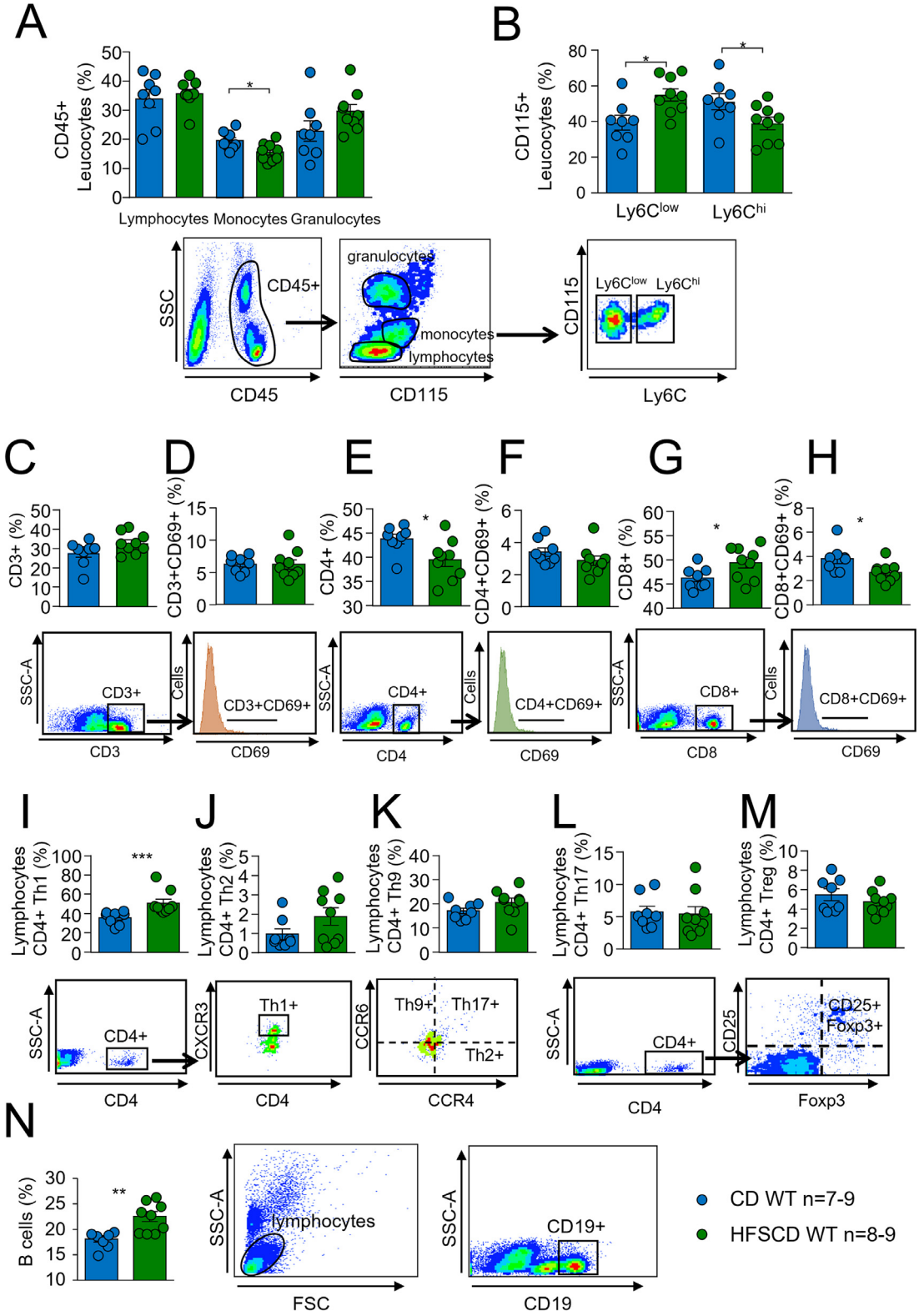

Fig. 6. Analysis of circulating leukocyte subsets in mice demonstrated an inflammatory profile in HFSCD-fed *WT* mice. (A) Percentage of circulating lymphocytes, monocytes and granulocytes identified in the CD45+ blood cell population by morphology and with the help of CD115+ monocyte marker. (B) CD45+CD115+Ly6C^{low} and CD45+CD115+Ly6C^{hi} monocyte subset percentages identified in the CD45+CD115+ cells in both groups of mice. Circulating percentages of (C) CD3+ T cells and their subsets (E) CD4+ and (G) CD8+ displayed as a percentage of CD3+ cells and their activated CD3+CD69+ (D), CD4+CD69+ (F) and (H) CD8+CD69+ cells referred to their total subsets. Circulating levels of (I) CD4+CXCR3+Th1, (J) CD4+CCR4+CCR6-Th2, (K) CD4+CCR4-CCR6+Th9, (L) CD4+CCR4+CCR6+Th17 and (M) CD4+CD25+Foxp3+ Treg cellular subpopulations displayed as percentages of the CD4+ population. (N) CD19+ B lymphocytes represented as percentage of total lymphocytes. Representative flow cytometry plots of the gating strategy for leukocytes, monocyte subsets, T and Th subpopulations in blood samples are shown below the corresponding quantifications. Data was represented as individual data points and with the mean±sem. Statistical analysis was performed using Studentś t test (A, B, K–N) and Mann-Whitney U test (C–H, I, J) ($^{*}P<.05$, $^{**}P<.01$ and $^{***}P<.001$).

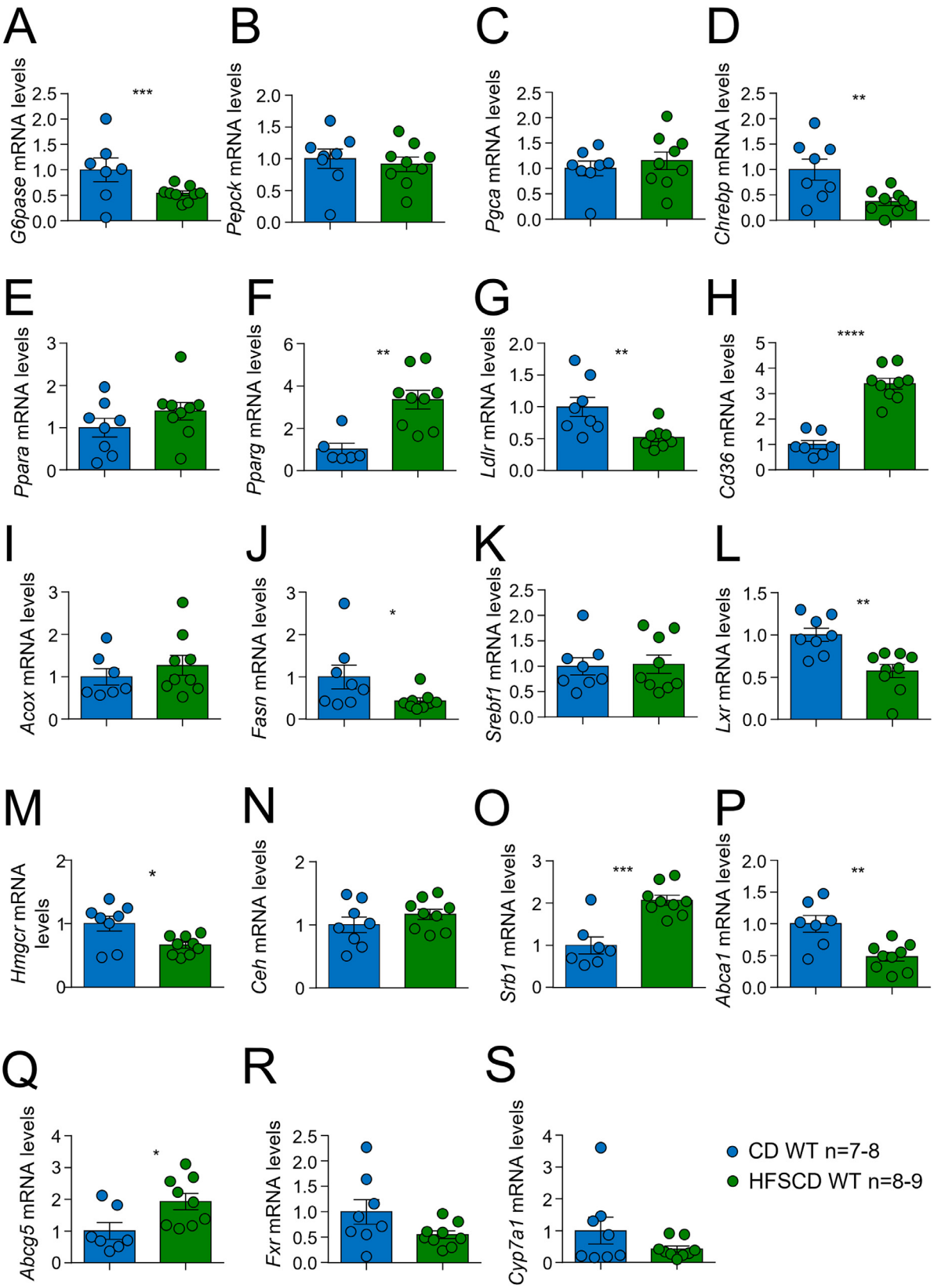

Fig. 7. *WT* mice fed with the HFSCD for 16 weeks, presents deranged hepatic metabolic gene expression. mRNA levels of (A) *G6pase*, (B) *Pepck*, (C) *Pgca*, (D) *Chrebp*, (E) *Ppara*, (F) *Pparg*, (G) *Ldlr*, (H) *Cd36*, (I) *Acox*, (J) *Fasn*, (K) *Srebf1*, (L) *Lxr*, (M) *Hmgcr*, (N) *Ceh*, (O) *Srb1*, (P) *Abca1*, (Q) *Abcg5*, (R) *Fxr*, and (S) *Cyp7a1*. mRNA levels were normalized to endogenous *Cyclophilin* expression and relativized to *WT* mouse levels. Data was represented as individual data points and with the mean±sem. Statistical analysis was performed using Studentś t test (A–D, E, H, K–O, Q–S) and Mann-Whitney U test (B, F, G, I, J, P). (*$P<.05$, **$P<.01$***, $P<.001$ and ****$P<.0001$).

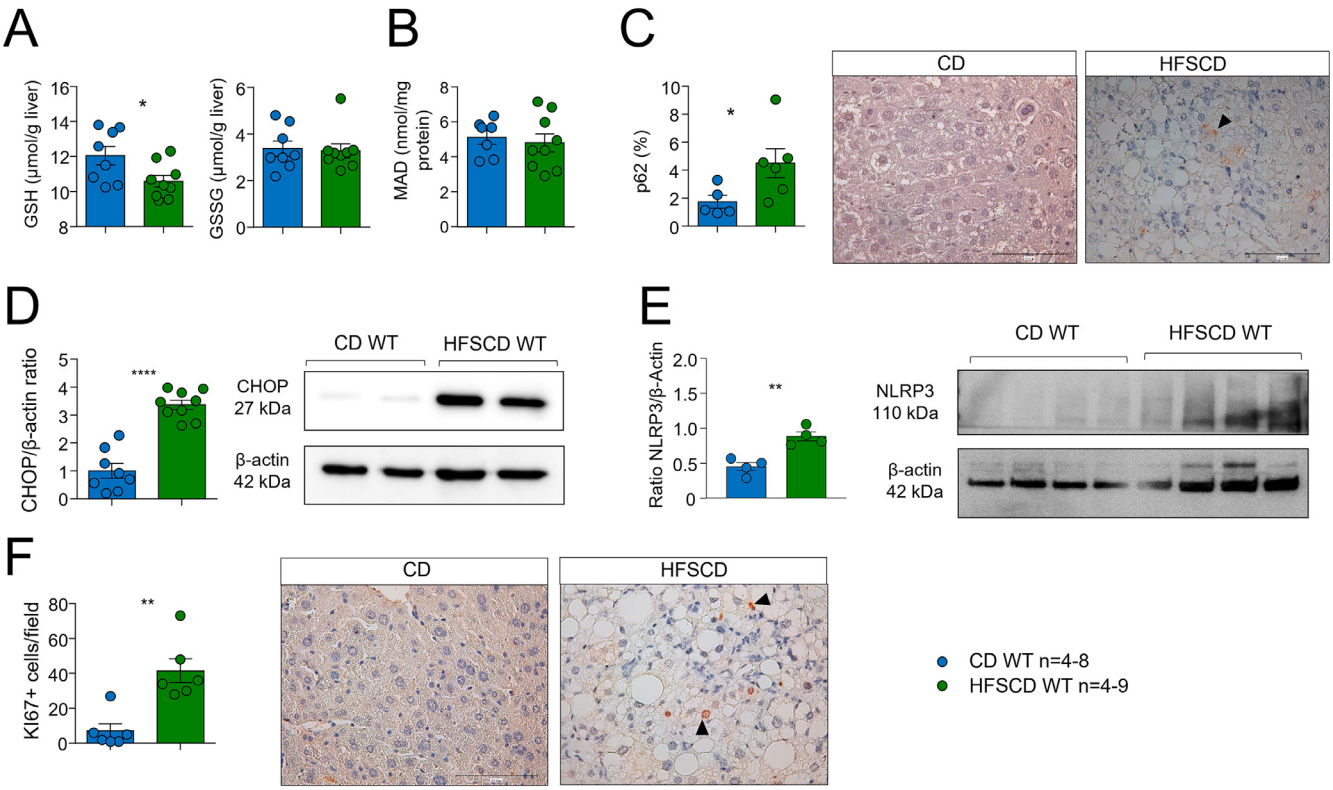

Fig. 8. The feeding of WT mice with the HFSCD produced important changes in hepatic autophagy, oxidative and ER stress and proliferation. Hepatic content of (A) reduced glutathione (GSH), oxidized glutathione (GSSG) and (B) MDA in both mouse groups. (C) Content of p62 protein, measured as relative area to tissue area, in hepatic cross-sections from *WT* mice fed control and HFSCD. (D) CHOP protein and (E) NLRP3 protein levels determined by western blot analysis in both mouse groups. (F) Number of proliferant Ki67+ cells (expressed as number of cells/ field) in hepatic cross-sections from both mouse groups. Representative images of the immunohistochemistry and of the blots used for the quantifications for CD- and HFSCD-fed mice are shown below the graphs. Protein levels were relativized to β-actin protein levels. Representative blots of the quantifications are shown for both mouse groups. Data was represented as individual data points and with the mean±sem. Statistical analysis was performed using Student́s t test (A–E) and Mann-Whitney U test (F) ($^{*}P<.05$, $^{**}P<.01$ and $^{****}P<.0001$).

and 1.25% of cholesterol to feed WT mice for 16 weeks will induce advanced NAFLD. Advanced NASH with fibrosis and inflammation was observed in HFSCD-fed WT mice hence confirming the presence of advanced disease. These mice also developed steatosis, hepatic damage, increased NAS score and augmented hepatic proliferation. Metabolic determinations showed increased plasma cholesterol, reduced NEFA and unchanged triglycerides in HFSCD-fed mice. However, regardless of these plasmatic levels HFSCD-fed mice displayed a higher intrahepatic accumulation of free cholesterol, NEFA and triglycerides. Notwithstanding, these mice did not develop IR, metabolism carbohydrate metabolism derangement or adipose tissue expansion. In fact, HFSCD-fed mice displayed reduced *Leptin* mRNA levels and increased activated HSL along with reduced mesenteric fat percentage which together with intrahepatic accumulation of NEFA suggested enhanced lipolysis. Further analysis indicated an increase in intrahepatic total CD3+T and Th9 lymphocytes and inflammatory cytokines as well as a reduction in anti-inflammatory F4/80+CD206+ macrophages and Th2 lymphocytes in HFSCD-fed mice. Consistently, these mice displayed higher levels of circulating cytotoxic CD8+T and proinflammatory CD4+Th1 lymphocytes. Hepatic gene expression analysis was compatible with reduced gluconeogenesis and lipogenesis but increased hepatic fatty acid and cholesterol uptake and accumulation which was in the line of the augmented intrahepatic lipid content in HFSCD-fed mice. Of note, development of disease also progressed with reduced antioxidant capacity, hepatic autophagy and CHOP protein levels suggesting ER stress possibly induced by the cholesterol overload. Analysis of the MAPK signaling pathways demonstrated increased ERK activation, but not JNK or p38. These results indicate that 16 weeks HFSCD-feeding in mice induces advanced NAFLD steatosis with fibrosis and inflammation along with ERK activation, enhanced apoptosis, and deficient autophagy.

NAFLD associated with IR, adiposity, dyslipidemia, and metabolic syndrome has been induced using diverse dietary regimens containing different percentages of sugar and fat and feeding times of at least 16-20 weeks. However, these diets fail to reproduce inflammation and fibrosis [17]. By contrary, inflammation, oxidative stress, and fibrosis are achieved in the methionine choline deficient (MCD) diet although this diet provokes an irreversible hepatoxicity among others [10]. A more clinically relevant alternative is the addition of cholesterol to the diet by using the so-called atherogenic or western diets [10]. These high cholesterol-containing diets can be clinically relevant as these recapitulate key features of critic stages of human NAFLD such as hepatic fibrosis and inflammation.

Previous studies by us employing WT (C57BL) mice treated with a 0.75% cholesterol-containing diet, with 10.8% of fat without sugar, produced glucose intolerance, insulin resistance (IR) and fatty liver [15,18]. Despite the diet produced a moderate degree of steatosis with a NAS score around two, systemic and hepatic inflammation were specially increased suggesting a cholesterol-mediated activation of inflammatory pathways [15]. The present diet, containing high sucrose and fat percentages and a 1,25% of cholesterol, provoked severe inflammation, fibrosis, a high NAS score and intrahepatic accumulation of cholesterol and NEFA.

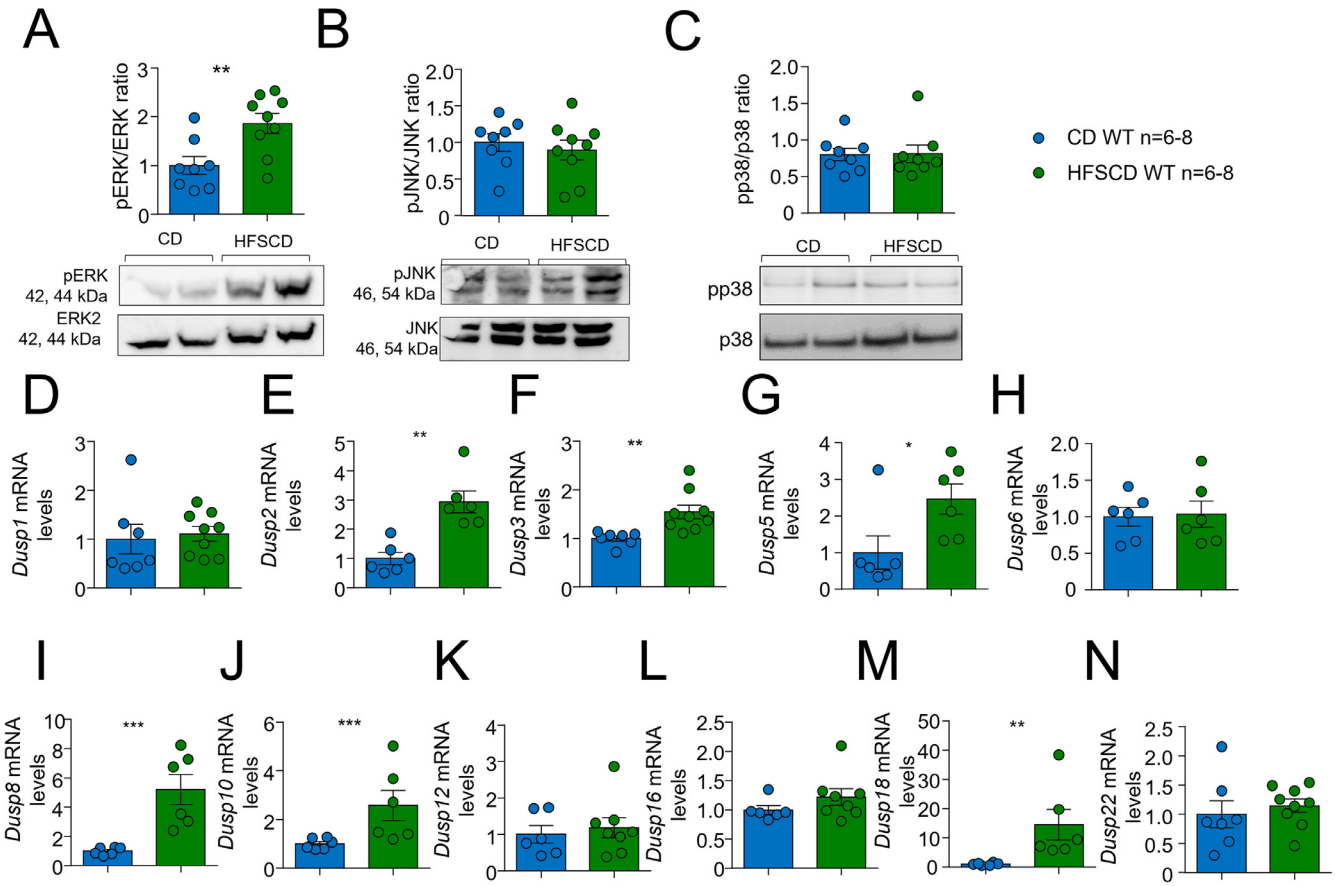

Fig. 9. HFSCD feeding in *WT* mice induced alteration of MAPK signaling cascades and phosphatases. Protein levels of activated phosphorylated (A) ERK (pERK) (B) SAPK/JNK (pJNK) and (C) p38 (pp38) relativized to their unphosphorylated total protein levels determined by western blot analysis. mRNA levels of phosphatases (D) *Dusp1*, (E) *Dusp2*, (F) *Dusp3*, (G) *Dusp5*, (H) *Dusp6*, (I) *Dusp8*, (J) *Dusp10*, (K) *Dusp12*, (L) *Dusp16*, (M) *Dusp18* and (N) *Dusp22*. Representative blots are shown for the phosphorylated and unphosphorylated forms of the kinases. mRNA levels were normalized to endogenous *Cyclophilin* expression and relativized to *WT* mouse levels. Data was represented as individual data points and with the mean±sem. Statistical analysis was performed using Studentś t test (A–D, E, F, H–K, N) and Mann-Whitney U test (G, L, M) (*$P<.05$, **$P<.01$ and ***$P<.001$).

Advantages seen in the present model were an accumulation of intrahepatic immune cells, such as Th9 mechanistically bound to fibrotic mechanisms [19], and changes in the reduced hepatic anti-inflammatory macrophages recently described as key determinants in human NASH and hepatic injury [20,21]. Consequently, HFSCD-fed mice showed increased hepatic expression of inflammatory cytokines and elevated circulating levels of proresolutory CD115+Ly6C^{low} monocytes owing to a lower hepatic infiltration of these [21]. Notably, Th9 are known to trigger inflammation and autoimmunity [22], induce fibrosis and associate with the progression of NASH [23]. Interestingly, *Rorc* expression levels were reduced which can relate with the prevalence of Th9 since *Rorc*-/- deficient T cells can acquire Th9 phenotype by increasing IL9 secretion [24]. Additionally, these changes were accompanied by a reduction of Th2, which could be the source of augmented Th9 [23]. Consequently, antibodies against IL9 ameliorate hepatic inflammation and NASH in CCl4-induced hepatic injury [25] which underlies a new possible avenue for hepatic fibrosis treatment.

The examination of circulating immune subsets supported a higher inflammatory status in HFSCD-fed mice. These displayed elevated Th1 lymphocytes, cytotoxic CD8+T cells and CD19+B cells circulating inflammatory parameters highly relevant in the NAFLD-NASH transition [26] and fibrotic stages [27,28]. All these findings indicate that the present dietary regimen generates is suitable and appropriate mouse model to study immune cell-mediated fibrotic NASH.

Advanced fibrotic stage in HFSCD-fed mouse model was evidenced by a higher hepatic contents of collagen, connective tissue, SM-α-actin and augmented mRNA levels of fibrotic *Tgfb1* and *Timp1* genes, determinant in NASH [29], suggesting a possible activation of HSC towards myofibroblasts. These results are consistent with the above results given that proinflammatory macrophage depletion associates with *Timp1* and *Tgfb1* and decreased fibrosis [21]. It should be noted that, in our previous investigations mice treated for the same period of time with a diet with a 10.8% total fat, 0.75% cholesterol, and no sugar, the levels of fibrosis were indistinguishable from CD-fed mice and accordingly, no changes in fibrotic genes were seen [15]. Therefore, the comparison of both studies indicates that the diet explored in this study, with 41.5% of sugar, 21% of fat and 1.25% of cholesterol, activates fibrotic genes.

Intrahepatic lipid accumulation was consistent with the transcriptomic data showing elevated *Cd36, Srb1* and *Abca1* as well as reduced *Abcg5* which would facilitate the hepatic uptake and retention of cholesterol and NEFA. In addition, augmented expression of the transporter *Cd36* has been seen in mice and human NASH while other investigations have reported NAFLD in mice that overexpress CD36 [20]. Altogether suggest that one of the mechanisms induced by the present dietary regimen could be the accumulation of cholesterol. Nevertheless, this hypothesis cannot be confirmed in this investigation which has the limitation of not making a proper comparison with cholesterol-free diets and future experiments should be performed in this direction.

Additional changes observed in HFSCD-fed mice were elevated hepatic mRNA levels of *Pparg* which induces a hepatic adipogenic program to create lipid droplets as a fatty acid storage [21]. However, hepatic gene expression of *Lxr, Chrebp* and *Srebf1c* genes which regulate glycolytic and lipolytic genes were diminished and this was consistent with a reduction in hepatic *Hgmcr* and *Fasn* mRNA levels.

HFSCD-fed mice did not develop glucose intolerance, IR or adiposity which are associated with enhanced lipid synthesis. In fact, HFSCD-fed mice displayed reduced body weight, mesenteric fat percentage and leptin production which also suggest smaller adipocyte size [30]. Notably, low leptin levels agree with a steatogenic phenotype as this hormone acts as an anti-steatotic signal by preventing lipid accumulation [31]. Consistently, leptin infusion prevents hepatic steatosis in both ob/ob and lipodystrophic mice and its administration is recommended in hypoleptinemic NAFLD patients [31]. These findings along with the intrahepatic accumulation of NEFA suggested enhanced lipolysis and flux of fatty acids from adipose tissue in HFSCD-fed mice. Indeed, activated HSL and *Perilipin* gene expression, which provides docking site for lipases in lipid droplets, were augmented in HFSCD-fed *WT* mice. Our results are similar to those observed in the MCD, in which the lack of adiposity is attributed to a hyper catabolism promoted by a sympathetic activity on adipose tissue and increased hepatic delivery of fatty acids to compensate for deficient hepatic VLDL secretion [32]. However, we cannot confirm impaired VLDL secretion as we did not specifically address this pathway. Given all these findings intrahepatic lipid accumulation in the HFSCD-fed mice is more plausible attributed to excessive fatty acid influx from adipose tissue rather than to an elevation in the *de novo* lipogenesis because the expression of genes of the lipid biosynthetic processes were reduced.

HFSCD-fed mice also displayed reduced antioxidative potential although oxidized lipids remained unchanged. Notwithstanding, mice developed ER-stress, subsequent inflammation and fibrosis as mentioned above. Moreover, inflammasome activation analysis, which is a main driver of NASH fibrosis [33] and a risk for the occurrence of cirrhosis and HCC [28], showed elevated NLRP3 marker protein in HFSCD-fed mice. Interestingly, intrahepatic free cholesterol positively correlated with CD3+ T cells and inversely correlated with anti-inflammatory macrophages suggesting a causal relationship between free cholesterol and inflammation.

Persistent high cholesterol levels are associated with ER stress by activating the UPR response [34], which leads to an inhibition of protective autophagy [35] and to an increased apoptosis [36]. Consistent with these, severity of NASH in HFSCD-fed mice was accompanied by increased levels of p62, which pointed to a deficient autophagy, and of CHOP, which is an ER-induced apoptosis marker. Notably, although autophagy is activated as a protective mechanism at early stages of NAFLD, the process is inhibited in advanced NASH [37]. Moreover, CHOP has been located as a protein at the cross-roads of autophagy and apoptosis which is activated in a PERK-dependent manner upon persistent metabolic ER stress such as amino acid privation [38] or HCC [39].

ER-stress has also been related with the three MAPK activation pathways including JNK, p38 and ERK [40] whose activation in macrophages can be induced by free cholesterol loading. In our study, ERK activation was augmented in HFSCD-fed mice in the line of studies describing the implication of the ERK pathway in obesity [41], in obesity-induced NAFLD [42] and in fatty liver through repression of fatty acid oxidation by PPARα inhibition [43]. Moreover, ERK activation aligns well with enhanced fibrosis in HFSCD mice and it has been associated with hepatic fibrosis through the proliferation and activation of PDGFβ-induced HSC [44]. Notably, the increased content of Th9 cells in HFSCD mice could be the triggering cell-type of fibrosis because other studies have shown that Th9 cells promote hepatic fibrosis by activating HSC in an ERK-dependent manner in mouse models of CCl4-induced hepatic injury [19]. Notwithstanding, other investigations reported aggravated fatty liver in mice with specific hepatic ERK2 deficiency [45]. The increased activation of the ERK pathway coincided with a higher number of proliferative cells in liver consistent with the ERK role in cell proliferation and differentiation [46]. Analysis of mRNA expression levels of DUSP/MKP phosphatases which modulate activation of the MAPK, revealed augmented levels of *Dusp5, Dusp*2, *Dusp3, Dusp*10 and *Dusp18*, all of which can potentially modulate ERK activation. Of these, protective functions against NAFLD and liver damage have been attributed to *Dusp10* and *Dusp3* through different mechanisms [47–48]. On the other hand, transcriptomic analysis have shown increased *Dusp5* and *Dusp18* in humans with liver damage, *Dusp5* expression is increased via ER stress [49] and *Dusp18* has been associated with HCC [50].

In our study, no major changes were seen in the activation levels of JNK despite this has been seen in mouse models of fatty liver, obesity and in HFD-fed mice by mechanisms that promote lipid accumulation, and activation of HSC and macrophages [51]. Similarly, the stress-MAPK p38 activation remained unchanged despite being associated with both protection and promotion of hepatic dysfunction [42].

In summary, the results obtained here indicate that the treatment with a HFSCD for 16 weeks generates a mouse model of NASH with advanced fibrosis and an imbalance of intrahepatic immune cells, hence recapitulating human disease severity. Specifically, the study provides evidence of intrahepatic free cholesterol accumulation which, through a reduction in resolutory macrophages, could promote ER stress-induced activation of the inflammasome. In addition, the liver of this mouse model of NASH was characterized by a reduction of intrahepatic Th2 cells and an accumulation of Th9 cells along with ERK activation which entails a potential mechanism for progression of fibrotic NASH induced by free cholesterol accumulation. Therefore, the use of this overnutrition-induced mouse model provides new opportunities for a better comprehension of immune cell-mediated fibrosis and to evaluate therapeutic targets for the treatment of advanced fibrotic NASH.

Funding

This study was supported by the Carlos III Health Institute (PI22/00062 and PI19/00169 to H.G.-N. and S.M.-H.), CIBERDEM (CB07/08/0043) and the European Regional Development Fund (FEDER). MA-B is a predoctoral fellow (FI20/00017) of the Carlos III Health Institute. GH-G was supported by a predoctoral program (FPU20/04916) of the Ministry of Universities. AV, AH-C and SM-V received salary from Proyecto Paula, and from the GenT Excellence program (CDEI-04-20-B of the GVA). The funders had no role in the design, analysis and reporting of the study.

Research data for this article

Data is available upon reasonable request to the corresponding author.

Declaration of competing interest

None.

CRediT authorship contribution statement

Alida Taberner-Cortés: Writing – original draft, Validation, Software, Methodology, Investigation, Formal analysis, Data curation, Conceptualization. **María Aguilar-Ballester:** Writing – review & editing, Writing – original draft, Methodology, Investigation, Formal analysis, Data curation, Conceptualization. **Elena Jiménez-Martí:** Writing – review & editing, Validation, Software, Resources, Project administration, Methodology, Data curation. **Gema Hurtado-Genovés:** Writing – review & editing, Software, Methodology, Formal analysis. **Rosa M. Martín-Rodríguez:** Writing – review & editing, Resources, Methodology, Investigation, Conceptualization. **Andrea Herrero-Cervera:** Writing – review & editing, Software, Methodology, Investigation. **Ángela Vinué:** Writing – review & editing, Resources, Methodology, Investigation. **Susana Martín-Vañó:** Project administration, Methodology, Formal analysis, Data curation. **Sergio Martínez-Hervás:** Writing – review & editing, Writing – original draft, Supervision, Funding acquisition, Conceptualization. **Herminia González-Navarro:** Writing – original draft, Validation, Supervision, Funding acquisition, Data curation, Conceptualization.

Acknowledgments

We thank G. Herrera for flow cytometry, A. Díaz for help with animal experimentation and N. Cabedo for the HPLC platform analysis (University of Valencia).

Supplementary materials

Supplementary material associated with this article can be found, in the online version, at doi:10.1016/j.jnutbio.2024.109711.

References

[1] Asrani SK, Devarbhavi H, Eaton J, Kamath PS. Burden of liver diseases in the world. J Hepatol 2019;70:151–71. doi:10.1016/J.JHEP.2018.09.014.
[2] Paik JM, Golabi P, Younossi Y, Mishra A, Younossi ZM. Changes in the global burden of chronic liver diseases from 2012 to 2017: the growing impact of NAFLD. Hepatology 2020;72:1605–16. doi:10.1002/HEP.31173.
[3] Allen AM, Therneau TM, Larson JJ, Coward A, Somers VK, Kamath PS. Nonalcoholic fatty liver disease incidence and impact on metabolic burden and death: a 20 year-community study. Hepatology 2018;67:1726–36. doi:10.1002/HEP.29546/SUPPINFO.
[4] Muoio DM, Newgard CB. Mechanisms of disease: molecular and metabolic mechanisms of insulin resistance and β-cell failure in type 2 diabetes. Nat Rev Mol Cell Biol 2008;9:193–205. doi:10.1038/nrm2327.
[5] Hatting M, Tacke F. From NAFLD to HCC: is IL-17 the crucial link? Hepatology 2017;65:739–41. doi:10.1002/hep.28934.
[6] Gomes AL, Teijeiro A, Burén S, Tummala KS, Yilmaz M, Waisman A, et al. Metabolic inflammation-associated IL-17A causes non-alcoholic steatohepatitis and hepatocellular carcinoma. Cancer Cell 2016;30:161–75. doi:10.1016/j.ccell.2016.05.020.
[7] Ramadori P, Kam S, Heikenwalder M. T cells: Friends and foes in NASH pathogenesis and hepatocarcinogenesis. Hepatology 2022;75:1038–49. doi:10.1002/hep.32336.
[8] Yang JD, Hainaut P, Gores GJ, Amadou A, Plymoth A, Roberts LR. A global view of hepatocellular carcinoma: trends, risk, prevention and management. Nat Rev Gastroenterol Hepatol 2019;16:589–604. doi:10.1038/s41575-019-0186-y.
[9] Dulai PS, Singh S, Patel J, Soni M, Prokop LJ, Younossi Z, et al. Increased risk of mortality by fibrosis stage in nonalcoholic fatty liver disease: systematic review and meta-analysis. Hepatology 2017;65:1557–65. doi:10.1002/hep.29085.
[10] Nevzorova YA, Boyer-Diaz Z, Cubero FJ, Gracia-Sancho J. Animal models for liver disease: a practical approach for translational research. J Hepatol 2020;73:423–40. doi:10.1016/j.jhep.2020.04.011.
[11] Arguello G, Balboa E, Arrese M, Zanlungo S. Recent insights on the role of cholesterol in non-alcoholic fatty liver disease. Biochim Biophys Acta - Mol Basis Dis 2015;1852:1765–78. doi:10.1016/j.bbadis.2015.05.015.
[12] Hagström H, Nasr P, Ekstedt M, Hammar U, Stål P, Hultcrantz R, et al. Fibrosis stage but not NASH predicts mortality and time to development of severe liver disease in biopsy-proven NAFLD. J Hepatol 2017;67:1265–73. doi:10.1016/J.JHEP.2017.07.027.
[13] Vinué Á, Herrero-Cervera A, González-Navarro H. Understanding the impact of dietary cholesterol on chronic metabolic diseases through studies in rodent models. Nutrients 2018;10: 939. doi:10.3390/NU10070939.
[14] Vinué Á, Navarro J, Herrero-Cervera A, García-Cubas M, Andrés-Blasco I, Martínez-Hervás S, et al. The GLP-1 analogue lixisenatide decreases atherosclerosis in insulin-resistant mice by modulating macrophage phenotype. Diabetologia 2017;60:1801–12. doi:10.1007/s00125-017-4330-3.
[15] Herrero-Cervera A, Vinué Á, Burks DJ, González-Navarro H. Genetic inactivation of the LIGHT (TNFSF14) cytokine in mice restores glucose homeostasis and diminishes hepatic steatosis. Diabetologia 2019;62:2143–57. doi:10.1007/s00125-019-4962-6.
[16] Folch J, Lees M, Sloane Stanley GH. A simple method for the isolation and purification of total lipides from animal tissues. J Biol Chem 1957;226:497–509. doi:10.1016/S0021-9258(18)64849-5.
[17] Ibrahim SH, Hirsova P, Malhi H, Gores GJ. Animal models of nonalcoholic steatohepatitis: eat, delete, and inflame. Dig Dis Sci 2016;61:1325–36. doi:10.1007/s10620-015-3977-1.
[18] Andrés-Blasco I, Herrero-Cervera A, Vinué Á, Martínez-Hervás S, Piqueras L, Sanz MJ, et al. Hepatic lipase deficiency produces glucose intolerance, inflammation and hepatic steatosis. J Endocrinol 2015;227:179–91. doi:10.1530/JOE-15-0219.
[19] Guo X, Cen Y, Wang J, Jiang H. CXCL10-induced IL-9 promotes liver fibrosis via Raf/MEK/ERK signaling pathway. Biomed Pharmacother 2018;105:282–9. doi:10.1016/j.biopha.2018.05.128.
[20] Chan MM, Daemen S, Beals JW, Terekhova M, Yang BQ, Fu CF, et al. Steatosis drives monocyte-derived macrophage accumulation in human metabolic dysfunction-associated fatty liver disease. JHEP Reports Innov Hepatol 2023;5:100877. doi:10.1016/j.jhepr.2023.100877.
[21] Kazankov K, Jørgensen SMD, Thomsen KL, Møller HJ, Vilstrup H, George J, et al. The role of macrophages in nonalcoholic fatty liver disease and nonalcoholic steatohepatitis. Nat Rev Gastroenterol Hepatol 2019;16:145–59. doi:10.1038/s41575-018-0082-x.
[22] Son A, Meylan F, Gomez-Rodriguez J, Kaul Z, Sylvester M, Falduto GH, et al. Dynamic chromatin accessibility licenses STAT5- and STAT6-dependent innate-like function of T(H)9 cells to promote allergic inflammation. Nat Immunol 2023;24:1036–48. doi:10.1038/s41590-023-01501-5.
[23] Kaplan MH. The transcription factor network in Th9 cells. Semin Immunopathol 2017;39:11–20. doi:10.1007/s00281-016-0600-2.
[24] Purwar R, Schlapbach C, Xiao S, Kang HS, Elyaman W, Jiang X, et al. Robust tumor immunity to melanoma mediated by interleukin-9-producing T cells. Nat Med 2012;18:1248–53. doi:10.1038/nm.2856.
[25] Qin S, Lu D, Guo X, Luo W, Hu B, Huang X, et al. A deleterious role for Th9/IL-9 in hepatic fibrogenesis. Sci Rep 2016;6:18694. doi:10.1038/srep18694.
[26] Wolf MJ, Adili A, Piotrowitz K, Abdullah Z, Boege Y, Stemmer K, et al. Metabolic activation of intrahepatic CD8+ T cells and NKT cells causes nonalcoholic steatohepatitis and liver cancer via cross-talk with hepatocytes. Cancer Cell 2014;26:549–64. doi:10.1016/j.ccell.2014.09.003.
[27] Bruzzì S, Sutti S, Giudici G, Burlone ME, Ramavath NN, Toscani A, et al. B2-Lymphocyte responses to oxidative stress-derived antigens contribute to the evolution of nonalcoholic fatty liver disease (NAFLD). Free Radic Biol Med 2018;124:249–59. doi:10.1016/j.freeradbiomed.2018.06.015.
[28] Mao T, Yang R, Luo Y, He K. Crucial role of T cells in NAFLD-related disease: a review and prospect. Front Endocrinol (Lausanne) 2022;13:1–19. doi:10.3389/fendo.2022.1051076.
[29] Ding ZM, Xiao Y, Wu X, Zou H, Yang S, Shen Y, et al. Progression and regression of hepatic lesions in a mouse model of NASH induced by dietary intervention and its implications in pharmacotherapy. Front Pharmacol 2018;9:1–15. doi:10.3389/fphar.2018.00410.
[30] Zhang Y, Guo K-Y, Diaz PA, Heo M, Leibel RL. Determinants of leptin gene expression in fat depots of lean mice. Am J Physiol Regul Integr Comp Physiol 2002;282:R226–34. doi:10.1152/ajpregu.00392.2001.
[31] Polyzos SA, Kountouras J, Mantzoros CS. Leptin in nonalcoholic fatty liver disease: a narrative review. Metabolism 2015;64:60–78. doi:10.1016/j.metabol.2014.10.012.
[32] Rizki G, Arnaboldi L, Gabrielli B, Yan J, Lee GS, Ng RK, et al. Mice fed a lipogenic methionine-choline-deficient diet develop hypermetabolism coincident with hepatic suppression of SCD-1. J Lipid Res 2006;47:2280–90. doi:10.1194/jlr.M600198-JLR200.
[33] Ioannou GN, Haigh WG, Thorning D, Savard C. Hepatic cholesterol crystals and crown-like structures distinguish NASH from simple steatosis. J Lipid Res 2013;54:1326–34. doi:10.1194/jlr.M034876.
[34] Sozen E, Ozer NK. Impact of high cholesterol and endoplasmic reticulum stress on metabolic diseases: An updated mini-review. Redox Biol 2017;12:456–61. doi:10.1016/j.redox.2017.02.025.
[35] Rodriguez-Navarro JA, Kaushik S, Koga H, Dall'Armi C, Shui G, Wenk MR, et al. Inhibitory effect of dietary lipids on chaperone-mediated autophagy. Proc Natl Acad Sci U S A 2012;109:E705–14. doi:10.1073/pnas.1113036109.
[36] González-Rodríguez A, Mayoral R, Agra N, Valdecantos MP, Pardo V, Miquilena-Colina ME, et al. Impaired autophagic flux is associated with increased endoplasmic reticulum stress during the development of NAFLD. Cell Death Dis 2014;5:e1179. doi:10.1038/cddis.2014.162.
[37] Ding H, Ge G, Tseng Y, Ma Y, Zhang J, Liu J. Hepatic autophagy fluctuates during the development of non-alcoholic fatty liver disease. Ann Hepatol 2020;19:516–22. doi:10.1016/j.aohep.2020.06.001.

[38] B'Chir W, Maurin AC, Carraro V, Averous J, Jousse C, Muranishi Y, et al. The eIF2α/ATF4 pathway is essential for stress-induced autophagy gene expression. Nucleic Acids Res 2013;41:7683–99. doi:10.1093/nar/gkt563.
[39] Lei Y, Wang S, Ren B, Wang J, Chen J, Lu J, et al. CHOP favors endoplasmic reticulum stress-induced apoptosis in hepatocellular carcinoma cells via inhibition of autophagy. PLoS One 2017;12:e0183680. doi:10.1371/journal.pone.0183680.
[40] Darling NJ, Cook SJ. The role of MAPK signalling pathways in the response to endoplasmic reticulum stress. Biochim Biophys Acta - Mol Cell Res 2014;1843:2150–63. doi:10.1016/j.bbamcr.2014.01.009.
[41] Bi L, Chiang JYL, Ding WX, Dunn W, Roberts B, Li T. Saturated fatty acids activate ERK signaling to downregulate hepatic sortilin 1 in obese and diabetic mice. J Lipid Res 2013;54:2754–62. doi:10.1194/jlr.M039347.
[42] Lawan A, Bennett AM. Mitogen-activated protein kinase regulation in hepatic metabolism. Trends Endocrinol Metab 2017;28:868–78. doi:10.1016/j.tem.2017.10.007.
[43] Mooli RGR, Rodriguez J, Takahashi S, Solanki S, Gonzalez FJ, Ramakrishnan SK, et al. Hypoxia via ERK signaling inhibits hepatic PPARα to promote fatty liver. CMGH 2021;12:585–97. doi:10.1016/j.jcmgh.2021.03.011.
[44] Lee YA, Wallace MC, Friedman SL. Pathobiology of liver fibrosis: a translational success story. Gut 2015;64:830–41. doi:10.1136/gutjnl-2014-306842.
[45] Kujiraoka T, Satoh Y, Ayaori M, Shiraishi Y, Arai-Nakaya Y, Hakuno D, et al. Hepatic extracellular signal-regulated kinase 2 suppresses endoplasmic reticulum stress and protects from oxidative stress and endothelial dysfunction. J Am Heart Assoc 2013;2:1–18. doi:10.1161/JAHA.113.000361.
[46] Cui A, Ding D, Li Y. Regulation of hepatic metabolism and cell growth by the ATF/CREB family of transcription factors. Diabetes 2021;70:653–64. doi:10.2337/dbi20-0006.
[47] Tang P, Low HB, Png CW, Torta F, Kumar JK, Lim HY, et al. Protective function of mitogen-activated protein kinase phosphatase 5 in aging- and diet-induced hepatic steatosis and steatohepatitis. Hepatol Commun 2019;3:748–62. doi:10.1002/hep4.1324.
[48] Jacques S, Arjomand A, Perée H, Collins P, Mayer A, Lavergne A, et al. Dual-specificity phosphatase 3 deletion promotes obesity, non-alcoholic steatohepatitis and hepatocellular carcinoma. Sci Rep 2021;11:1–15. doi:10.1038/s41598-021-85089-6.
[49] Jo HJ, Yang JW, Park JH, Choi ES, Lim CS, Lee S, et al. Endoplasmic reticulum stress increases DUSP5 expression via PERK-CHOP pathway, leading to hepatocyte death. Int J Mol Sci 2019;20:4369. doi:10.3390/ijms20184369.
[50] Pu J, Qin Z, Fang Q, Huang Y, Lu Y, Li W, et al. Hypoxia-induced HIF1A activates DUSP18-mediated MAPK14 dephosphorylation to promote hepatocellular carcinoma cell migration and invasion. Pathol Res Pract 2022;237:153955. doi:10.1016/j.prp.2022.153955.
[51] Nikolic I, Leiva M, Sabio G. The role of stress kinases in metabolic disease. Nat Rev Endocrinol 2020;16:697–716. doi:10.1038/s41574-020-00418-5.